AD NUMBER

AD831716

NEW LIMITATION CHANGE

TO

Approved for public release, distribution unlimited

FROM

Distribution authorized to U.S. Gov't. agencies and their contractors; Administrative/Operational Use; MAY 1967. Other requests shall be referred to Air Force Materials Lab., Wright-Patterson AFB, OH 45433.

AUTHORITY

AFML ltr, 7 Dec 1972

GEORGE SHOL

AFML-TR-67-232

STUDY OF MICROPLASTIC PROPERTIES AND DIMENSIONAL STABILITY OF MATERIALS

A. G. Imgram, R. E. Maringer, and F. C. Holden

Battelle Memorial Institute

TECHNICAL REPORT AFML-TR-67-232

May, 1967

Air Force Materials Laboratory
Directorate of Laboratories
Air Force Systems Command
Wright-Patterson Air Force Base, Ohio

83

NOTICE

AFML-TR-67-232

STUDY OF MICROPLASTIC PROPERTIES AND DIMENSIONAL STABILITY OF MATERIALS

A. G. Imgram, R. E. Maringer, and F. C. Holden

Battelle Memorial Institute

TECHNICAL REPORT AFML-TR-67-232

May, 1967

Air Force Materials Laboratory
Directorate of Laboratories
Air Force Systems Command
Wright-Patterson Air Force Base, Ohio

FOREWORD

This report was prepared by Battelle Memorial Institute, Columbus, Ohio under USAF Contract No. AF 33(615)5218. The contract was initiated under Project No. 7351 "Metallic Materials", Task No. 735103 "Unique Metallic Materials". The work was administered under the direction of the Air Force Materials Laboratory, Directorate of Laboratories with Lt. Fred Gurney and Mr. George Saul (MAMN) acting as project engineers.

The report covers work conducted during the period July 1966 - July 1967.

The manuscript was released by the authors 11 July 1967 for publication as an AFML Technical Documentary Report.

This technical report has been reviewed and is approved.

THOMAS D. COOPER
Chief, Processing &
Nondestructive Testing Br
Metals & Ceramics Division

ABSTRACT

Microyield stresses of 39-40 ksi for Ni-Span-C, 69-70 ksi for 440 C stainless steel, and 7.5 ksi for A 356 cast aluminum have been determined. Microyield stress tests are in progress for Ti-5Al-2.5Sn, beryllium, and aluminum oxide. Experiments have shown that residual strains of 20-40 μin./in. increase the microyield stress, but a small fraction of this increase is lost upon allowing the specimen to recover at room temperature for up to 24 hours. Electron microscope studies indicated that microplastic flow in Ni-Span-C is the result of dislocation generation at second phase particles in grain boundaries. For A 356 cast aluminum, the generation of interfacial dislocations at Mg_2Si particles appeared to be the controlling mechanism.

Experiments are being conducted to determine, and eventually minimize, the residual stresses introduced by machining in all of the materials being studied. In addition, the effects on dimensional stability of load and thermal cycling, and plastic strain are being investigated.

A prototype capacitor strain gage has been constructed. The design is currently being modified to eliminate slippage of the gage elements as the specimen is loaded and unloaded.

TABLE OF CONTENTS

TABLE OF CONTENTS
(Continued)

ILLUSTRATIONS

ILLUSTRATIONS
(Continued)

INTRODUCTION

This report summarizes the results obtained during the first year of a two-year study of the microplastic properties and dimensional stability of structural materials.

Increased accuracy and precision are becoming more important as industry demands greater reliability in the performance of precision devices. As an example, the requirements of missile and space systems have now reached the stage where minute inaccuracies can lead to failure of the mission. This has imposed extremely high requirements on the accuracy of the guidance system and its associated instrumentation.

It has been stated that, with continuing improvements in machining techniques, tolerances specified in microinches soon will be commonplace. As a consequence, dimensional changes of only a few microinches will become increasingly significant, not only to the present producers of precision instruments, but to a much broader segment of industry. The current needs of the aerospace industry for better information on the dimensional stability of materials thus lends impetus to studies in an area that will be vitally important to other industries within the next decade.

Dimensional instability of this order of magnitude until recently was of interest only to the manufacturers and users of reference standards such as gage blocks. In fact, only recently has the stability of reference standards themselves reached a point where dimensional changes of this order can be measured in a reliable manner.

The precision of many present-day instruments is already better than the stability of the materials from which they are made.

Further developments of instrumentation will be limited severely unless significant progress is made toward improving material stability.

Dimensional changes can be caused by both internal and external factors.

Some of the internal mechanisms that cause dimensional instability in metals are at least qualitatively well known. Probably the two more important of these are (1) metallurgical instability in the microstructural sense, and (2) the relaxation of residual stresses. Some of the more subtle metallurgical reactions that can cause dimensional changes are less well understood. These include the effects of ordering of interstitial and substitutional atoms, the effects of grain-boundary migration, and movements of magnetic domain walls. Some of the metallurgical mechanisms leading to dimensional changes are:

(1) Metals or alloys that do not undergo a phase change form the simplest class of material. The only apparent microstructural changes are in grain size, shape, and orientation. One metallurgical change which can cause small dimensional changes is ordering. Individual solute atoms often will tend to occupy specific positions in the solvent lattice relative to stress or magnetic vectors, or even relative to like or unlike atoms. Because these reactions are controlled by the diffusivity of the solute in question, the reaction rates are distinguished by a relatively strong temperature dependence. Small dimensional changes will follow changes in stress, magnetization, or possibly temperature. Such reactions can be responsible for warm-up times for oscillating devices, hysteresis behavior during the stress cycle, or time dependence <u>after</u> reaching some fixed new temperature.

(2) An alloy that rejects a second phase from solid solution (typical of the age-hardening alloy systems) will usually undergo a gradual change in volume. The rate of the reaction is dependent upon time and temperature and the degree of departure from phase equilibrium. The reaction also may be sensitive to applied stress, the application of vibrational energy, and the level of impurities in the alloy.

(3) A metal or alloy that undergoes a transformation from one allotropic form to another will change in volume. The change may be positive or negative, depending upon the relative specific volumes of the two phases. In steel, for example, the transformation from austenite to martensite results in a volume increase, the magnitude of which is dependent upon alloy composition.

(4) Combinations of the several mechanisms described above may occur concurrently. For example, a steel may exhibit simultaneously a positive volume change from the transformation of retained austenite and a negative volume change from the tempering of martensite. Thus, the net volume change may be positive, negative, or zero; it also may change from one to the other over a period of time as one mechanism becomes dominant over another.

Shape distortions introduced by the relaxation of residual stresses are somewhat more difficult to analyze. Residual stresses most frequently are introduced during fabrication or heat treatment and are characteristically nonuniform. Distortion then takes place through time-dependent plastic flow. The analysis of this problem is complicated by the fact that distortions in the microinch-per-inch range can result from residual-stress changes well below the present limits of experimental stress measurement. Further, present methods for the measurement of residual stresses are quantitatively useful only for sections of simple geometry. The stress distribution and consequent distortion of parts with more complex shapes can be predicted only qualitatively.

As was pointed out previously, both metallurgical and residual-stress mechanisms are operative in most cases; therefore, the gross dimensional change measured will be the sum of the two types of distortions. Under very special conditions, it may be possible to balance the two to obtain satisfactory dimensional stability, as has been done by the National Bureau of Standards in some of its gage-block studies. More usually, it will be necessary to reduce both the metallurgical instability

and the residual-stress levels to attain the necessary degree of dimensional stability.

In principle, methods for eliminating the two major sources of dimensional instability are known. Both mechanisms of instability are time and temperature sensitive. Metallurgical stability is promoted by approaching phase equilibrium, whereas residual stresses are reduced by stress-relief annealing. In practice, several difficulties exist: (1) the optimum procedures for attaining phase equilibrium and stress-relief annealing for a particular alloy may not be known, (2) the two may not be compatible with each other, and (3) other requirements (such as strength, hardness, or corrosion resistance) may require treatments that are not compatible with each other or with the equilibrating and stress-relief treatments. The influence of internal stresses and metallurgical changes on dimensional stability is determined by measuring the changes in length of specimens over a period of time.

Microplastic response to externally applied loads is frequently evaluated in terms of the microyield stress and microcreep limit tests. The microyield stress is defined as the minimum stress required to cause a permanent residual strain of 1 μin./in. The microcreep limit is similar to the microyield stress, but the test procedure is modified to detect time dependent microplastic flow.

This research program is designed to evaluate the microplastic properties and dimensional stability of selected structural materials suitable for construction of precision equipment. The dimensional stability of each material is being examined as a function of machining, load cycling, thermal cycling, and plastic deformation. All specimens

have been given a primary heat treatment to develop a characteristic microstructure. The results will be used to outline a processing sequence for maximum dimensional stability.

Efforts are being made to determine the basic mechanisms involved in microplastic flow and dimensional instability.

In addition to the mechanical-property studies, a phase of this research is directed toward the design and evaluation of a capacitor strain gage.

SUMMARY

The purpose of this research program is to evaluate the microplastic properties and dimensional stability of Ni-Span-C, 440 C stainless steel, A 356 cast aluminum, Ti-5Al-2.5Sn, beryllium, aluminum oxide, and the dimensional stability of a modified zirconium oxide (Zyttrite).

The average microyield stress (stress to cause residual strain of 1 μin./in.) and conventional tensile properties of Ni-Span-C, 440 C, and A 356 were found to be as follows:

Material	Microyield Stress, ksi	0.2% Offset Yield Stress, ksi	Ultimate Tensile Strength, ksi	Elongation, percent
Ni-Span-C	40	104	175	12
440 C	70	(a)	235	0
A 356	7.5	22	31	3

(a) Fracture before yielding

Difficulty was encountered in obtaining reliable microyield stress data for Ti-5Al-2.5Sn and aluminum oxide because of negative residual strain artifacts and brittle fracture respectively. Efforts are being made to circumvent these problems by using a capacitor strain gage for the Ti-5Al-2.5Sn and by redesigning the aluminum oxide specimens. A "high precision elastic limit" beryllium alloy has been ordered, and microyield stress tests will be conducted as soon as the material has been received.

Experiments have shown that residual strains of 20-40 μ in./in. significantly increase the microyield stress of 440 C stainless steel,

but a small fraction of this increase is lost upon allowing the specimens to recover at room temperature for up to 24 hours. Similar experiments will be conducted with some of the other materials being studied.

Electron microscope studies indicate that microyielding in Ni-Span-C is the result of dislocation generation at second phase particles in grain boundaries. For A 356, the generation of interfacial dislocations at Mg_2Si particles appeared to be the controlling mechanism.

Microcreep limit tests with Ni-Span-C and 440 C have shown that no significant time dependent microplastic flow occurs when specimens are held at load for up to 15 minutes at stresses of up to approximately twice the microyield stress. Therefore, dead weight loaded microcreep tests for longer periods will be substituted.

The dimensional stability of each of the materials is being evaluated as a function of residual stresses introduced by machining, plastic strain, and load and temperature cycling. Severe problems were encountered in measuring the length of specimens to the required precision of 1 μ/in. Equipment and techniques were developed that solved most of these problems, and the planned experiments are now underway. To date, maximum residual stresses of 15 and 8 ksi have been determined in rough machined Ni-Span-C and 440 C respectively.

A prototype capacitor strain gage has been constructed for use in microstrain measurement. Preliminary evaluation indicated that the gage elements slip as the specimen is loaded and unloaded. The gage is currently being redesigned to eliminate the slippage, and will be used to determine the microyield stress of Ti-5Al-2.5Sn once it has been perfected.

EXPERIMENTAL PROCEDURES

All micromechanical property testing and precision length measurements were performed in a Sheffield Modulab in which the temperature is maintained at 68 ± 1/4 F.

Materials

Five metals and two ceramics have been selected for study. The five metals, along with their chemical analyses supplied by the vendors, are given in Table I.

Ni-Span-C is an age-hardenable iron-nickel alloy with an austenite matrix. Its modulus of elasticity can be maintained constant or varied over a given temperature range by controlling the thermo-mechanical processing history. This property has led to its use in a number of precision instrument applications.

440 C stainless steel is a high chromium, high-carbon iron-base alloy. It has a martensite matrix and is age hardenable. This steel offers a superior combination of high strength, wear resistance, and corrosion resistance, and is seeing increasing use as a bearing material.

Ti-5Al-2.5Sn is an all alpha, nonheat-treatable titanium alloy offering moderate strength and high-fracture toughness. Fusion welds can provide the same strength and toughness as the base metal. These properties have led to considerable use in missile applications.

A 356 cast aluminum possesses good castability and better corrosion resistance than most other high-strength aluminum casting

TABLE I. CHEMICAL ANALYSIS

Element	Composition, wt%				
	Ni-Span-C[a]	440C Stainless Steel	Ti-5Al-2.5Sn	A 356 Cast Aluminum[b]	Beryllium
Al	0.30-0.80		5.0	Balance	
Mn	<0.80	0.42	0.006		Material on order
P	<0.04	0.016			
S	<0.04	0.012			
Si	<1.0	0.40		6.98	
Cr	4.9-5.75	17.43			
Ni	41.0-43.5	0.49			
Mo		0.48			
Zn				0.02	
Ti	2.2-2.75		Balance	0.21	
Fe	Balance	Balance	0.27	0.10	
Mg				0.36	
C	<0.06	1.4	0.023		
N			0.016		
O			0.19		
H			0.008		
Sn			2.6		

(a) Nominal Composition
(b) Ingot Analysis

alloys. Highest strength is achieved with permanent mold castings. It is widely used for precision castings where both weight and cost must be minimized.

Beryllium has a very low density and a high modulus of elasticity. This combination of properties makes beryllium exceptionally useful for structures such as gyroscopes or telescope mirrors that must be light in weight but provide high rigidity to applied loads.

Ni-Span-C, 440 C stainless steel, and Ti-5Al-2.5Sn were procured as wrought bar stock. A 356 aluminum was purchased in the form of pigs and was subsequently cast tinto tow leg "keel blocks" at Battelle. Specimen blanks were sliced from the legs which had a 1-inch cross section. A "high precision elastic limit" beryllium alloy has been ordered from Berylco. This material will be received in the form of rods machined from a powder metallurgy ingot. The test results on this material will complement micromechanical-property data on I-400 Brush Beryllium alloy being obtained by Battelle on a program for the NASA Goddard Space Flight Center.*

The two ceramics being evaluated are aluminum oxide and a modified form of zirconium oxide. A trial lot of aluminum oxide has been ordered and tested. A second lot has recently been ordered to evaluate an improved specimen deisgn for the tensile testing of brittle ceramics as will be discussed in a following section of this report. Zirconium oxide (Zyttrite) is a refractory oxide that has been recently developed by the Metals and Ceramics Division of the Air Force Materials Laboratory. The quantities of material currently available are extremely limited. At present, only two small samples have been received for a check of dimensional stability. Microplastic

* Contract NAS 5-10267

properties will be determined if additional material becomes available in the future.

Mechanical-Property Testing

Three different mechanical-property tests have been conducted as follows:

(1) Microyield stress:* stress required to cause a residual plastic strain of 1 μin./in.

(2) Microcreep limit: similar to microyield stress, but specimen is held at load for a predetermined period to permit time-dependent plastic deformation

(3) Conventional tensile properties: ordinary 0.2 percent offset yield stress, ultimate tensile strength, elongation, and reduction in area.

A full description of testing procedures and conditions is given in a following section of this report.

Specimen Preparation

Figure 1 gives the specifications of the specimens used for the determination of the above mechanical properties of the metals being studied. The specimens were first rough machined to 0.010 inch larger than final dimensions, and then heat treated to produce a microstructure characteristic of each alloy. After heat treatment, the specimens were finish machined to final specifications. Any distortion or surface contamination due to heat treatment was eliminated by the finish machining.

---

* Formerly denoted as the "precision elastic limit"

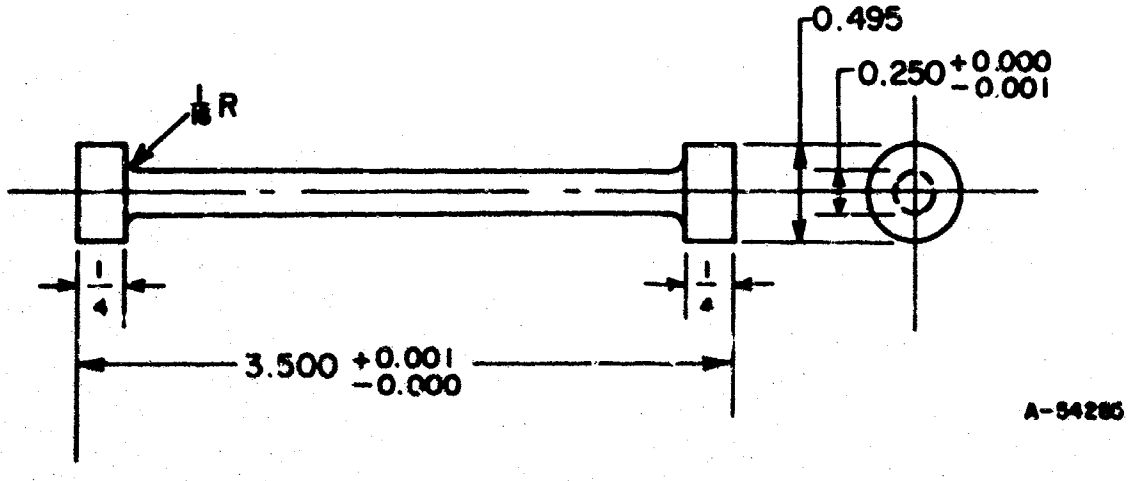

FIGURE 1. SPECIMEN FOR MICROPLASTIC PROPERTY, CONVENTIONAL TENSILE PROPERTY, AND LOAD AND THERMAL-CYCLE DIMENSIONAL-STABILITY TESTS

The heat treatments employed for each alloy are described in Table II. They are based on those recommended by MIT[1] for maximum dimensional stability. Microstructures of heat-treated material are shown in Figure 2.

The specimen design used for aluminum oxide was similar to that shown in Figure 1 with the exception that 30° chamfers were employed to provide a gradual transition of cross-sectional area between the loading shoulder and the test section.

Strain Gage Application

Three strain gages were applied to each specimen and were spaced 120° apart around the circumference.

Materials. The strain gages used in this study were SR-4, epoxy base, constantan foil gages, type FA-2SN-12S. The gage configuration is shown in Figure 3, and the manufacturer's specifications are given below:

Resistance, ohms	120.0 ± 0.2
Nominal Gage Factor	2.1 ± 1%
Grid Length, inch	0.25
Grid Width, inch	0.02

The temperature compensation of the gages was matched as closely as possible to the thermal expansion of each material as shown in Table III.

The adhesive used to apply the gages to all of the materials was BR-600, an epoxy cement with excellent stability and creep characteristics.

Specimen Preparation. Before gaging, approximately 10 mils was removed from the diameter of the gage length of each specimen

TABLE II. HEAT TREATMENTS

Alloy	Heat Treatment
Ni-Span-C	1-1/4 hr at 1800 F, water quench; 21 hr at 1250 F, air cool
440 C Stainless Steel	1/2 hr at 1900 F, oil quench, hold for 2 min; immerse in liquid nitrogen for 30 minutes;(a) 1 hr at 520 F, air cool
Ti-5Al-2.5Sn	1 hr at 1500 F in argon, furnace cool
A 356 Cast Al	16 hr at 1000 F, boiling water quench; 4 hr at 310 F, air cool
Beryllium	To be selected

(a) Recommended in Metals Handbook, Vol.II, to reduce retained austenite content

TABLE III. THERMAL EXPANSION AND STRAIN-GAGE COMPENSATION

Material	Coefficient of Thermal Expansion, μin./in./F	Gage Compensation, μin./in./F
A 356 Aluminum	11.5	13.0
Ni-Span-C	4.5	4.7
440 C Stainless Steel	5.6	6.0
Al_2O_3	4.0	3.0
Ti-5Al-2.5Sn	5.25	6.0

100X 4B247

a. Ni-Span-C

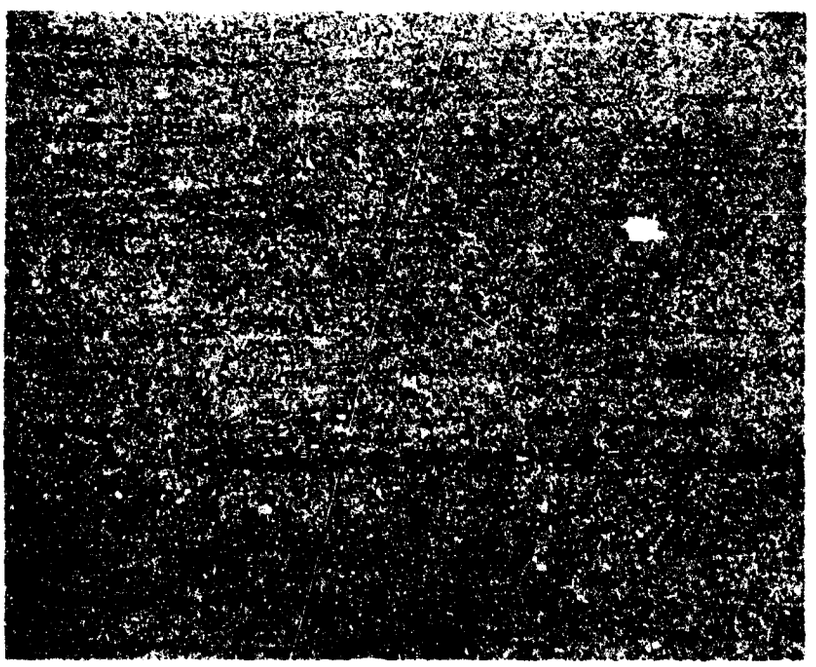

100X 4B243

b. 440C Stainless Steel

FIGURE 2. MICROSTRUCTURE OF HEAT-TREATED MATERIALS

4B245

c. A356 Cast Aluminum

FIGURE 2. (CONTINUED)

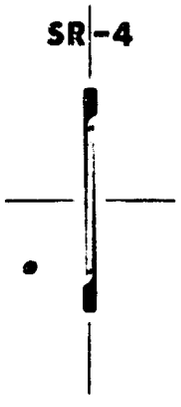

38141

FIGURE 3. STRAIN GAGE USED IN THIS STUDY

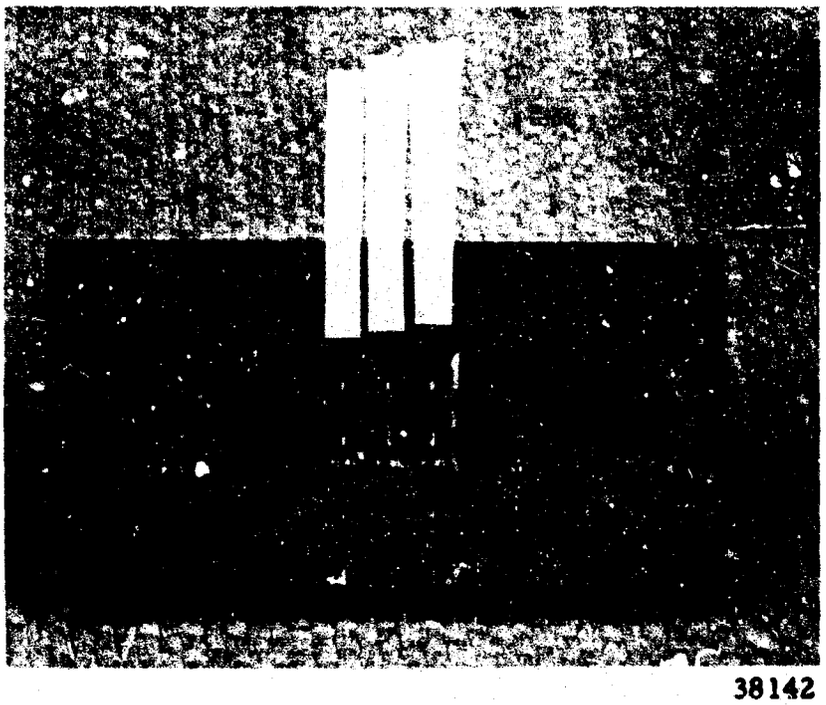

38142

FIGURE 4. STRAIN-GAGE ASSEMBLY ON GRID USED TO OBTAIN 120 DEGREE SPACING

(excluding the Al_2O_3) by chemical milling. The shoulders of the specimens were protected with Microwax Stop-off C-562. The solutions, temperatures, and techniques used for each material are given in Table IV.

Gage Application. The gage backing was first trimmed to a width of approximately 0.2 inch so that three of them would fit around the sample without overlapping. Each gage was then attached to a paper handling tab with a small piece of mylar tape. Three of these gages were then layed out on a grid as shown in Figure 4 to assure proper spacing for the 120° separation, and another piece of mylar tape was placed over the gages to hold their spacing. This assembly was then lifted from the grid and the excess tape was trimmed off.

At this point, the gage assembly was laid aside, and the specimen to be gaged was cleaned first by swabbing with acetone followed by washing with a "metal conditioner" (a weak acid solution) and finally by rinsing with neutralizer (ammonia). The gages in the assembly described above were also cleaned with the neutralizer.

A thin layer of cement was then applied to the gages and allowed to air dry for 5 minutes. The gage assembly was carefully aligned on the sample using a specially marked V-block and one end was tacked down with the tape. At this point, the specimen was lifted from the V-block and appeared as shown in Figure 5. The entire assembly was then wrapped securely around the sample smoothing each gage with thumb pressure. A silicone rubber pad and a thin aluminum plate were placed over each of the three gages and were held in place by a "hose clamp". The cement was then cured for 1 hour at 225 F.

TABLE IV. CHEMICAL MILLING PROCEDURES

Material	Solution	Etching Temperature	Technique
A 356 Al	100 grams sodium hydroxide in 500 cc water	115 F	Stir slowly
Ni-Span-C and 440 C Stainless	3 parts water 1 part hydrochloric acid	Room temp.	Make specimen an anode in an electolytic bath with a current density of 0.9 amps/cm^2
Ti-5Al-2.5Sn	60 parts lactic acid, 20 parts nitric acid, 20 parts hydrofluoric acid	Room temp.	Stir slowly
Al_2O_3	Not etched		

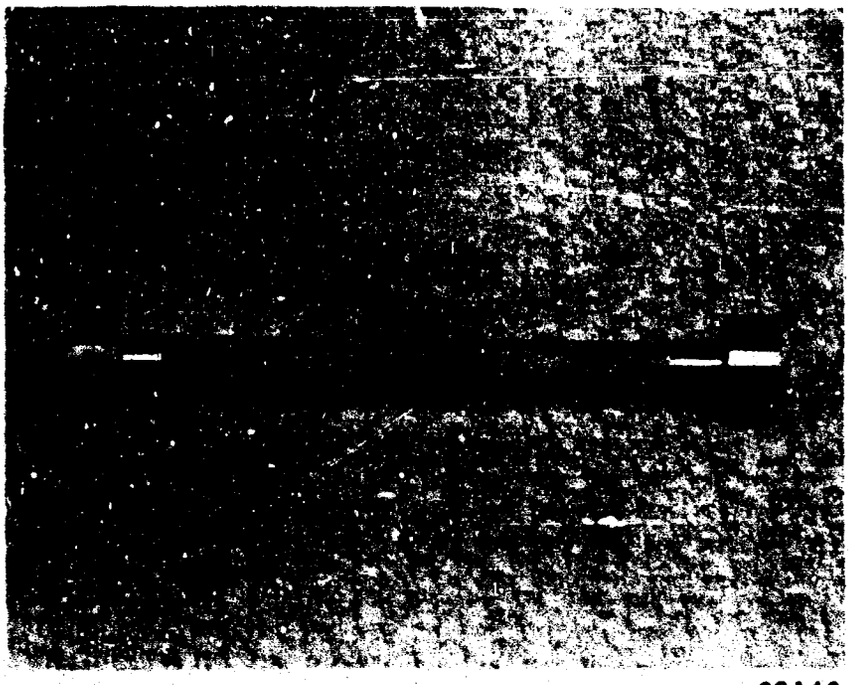

38143

FIGURE 5. STRAIN-GAGE ASSEMBLY READY TO WRAP AROUND SPECIMEN

After curing, the clamp and pads were removed and the tape was stripped off. A copper terminal strip on fiber-glass backing was installed near each tab using Eastman 910 contact cement. Both the terminal strips and gage tabs were tinned with 300 F solder. The lead wires (26 ga. stranded copper) were soldered to the terminal strips with a single strand of wire extending over to the gage tabs. The entire installation is shown in Figure 6. Gagecote #1, a solvent thinned resin, was applied as waterproofing prior to testing.

Testing Procedures

Microyield Stress. The microyield stress of each material was determined by loading specimens to successively higher stress levels and measuring the residual strain after removal of the load from each stress increment. The load was relaxed immediately upon attainment of the desired stress levels. Each specimen was loaded to stress levels sufficient to cause 20-40 μin./in. residual strain.

All tests were performed in an Instron Testing Machine. A photograph of the load train is shown in Figure 7. The load was applied to the specimens through a universal joint and a thrust bearing to minimize bending and torsion moments. The specimen loading shoulders were gripped in a spherical seat employing a split-collar as shown in Figure 8. Specimens were loaded using a constant cross-head speed of 2.0 inches per minute.

Prior to actual testing, a small load (approximately 25 pounds) was applied to the specimen, and eccentricity of loading was minimized by adjusting the specimen and load train until the strains on the three

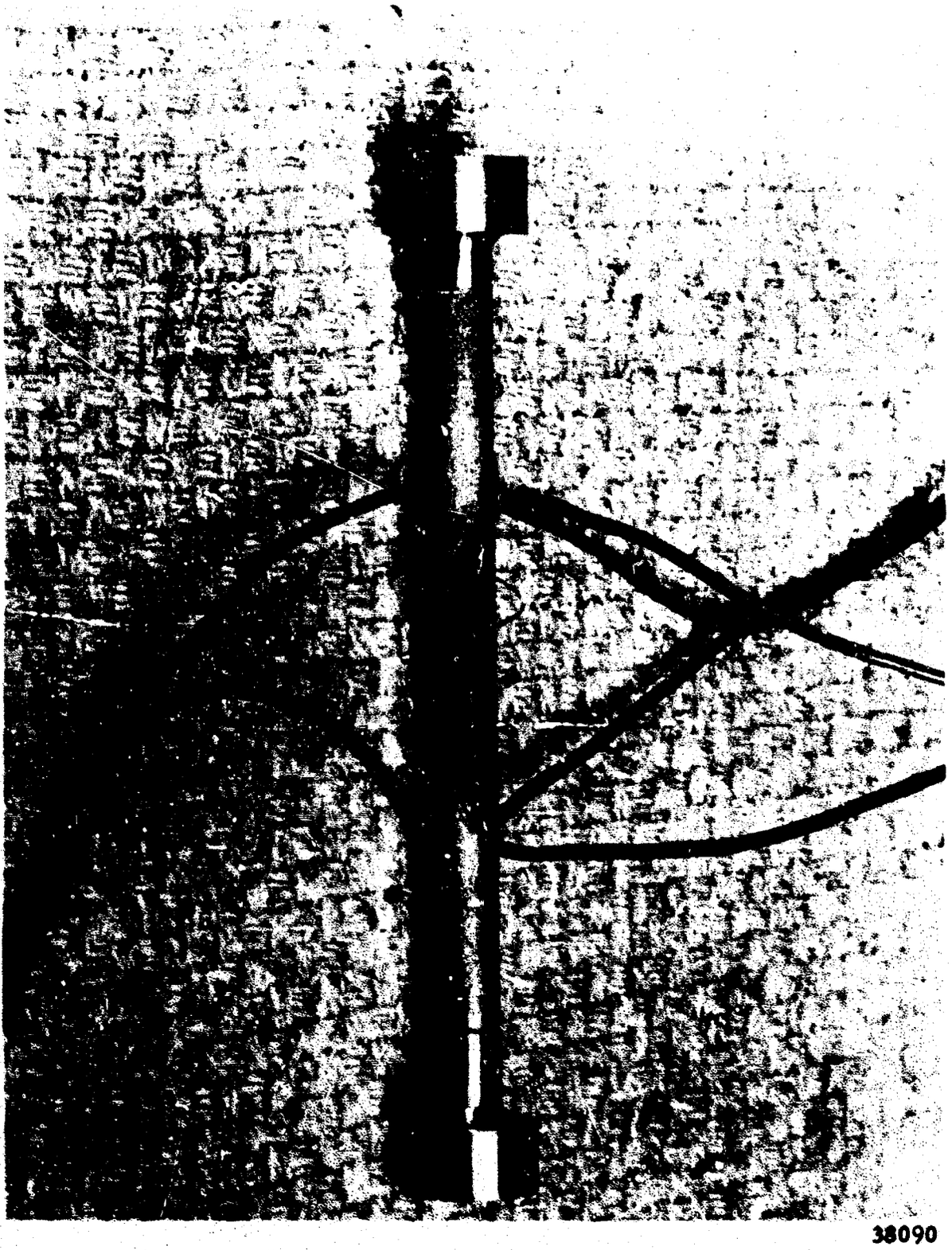

38090

FIGURE 6. COMPLETED INSTALLATION PRIOR TO WATERPROOFING

FIGURE 7. MICROMECHANICAL PROPERTY TESTING LOAD TRAIN

33140

FIGURE 8. SPHERICAL SEAT

gages were as nearly identical as possible. Some eccentricity always remained and was probably largely due to slight bending of the specimens and/or nonparallelism of the loading shoulders.

Residual strain measurements were made by determining the strain on each of the three gages individually with a BLH Strain Indicator. This instrument was modified at the factory to increase its sensitivity. The gages and strain indicator are capable of measuring residual strains with a sensitivity 0.1 μin./in. Each gage was wired into a full bridge circuit external from the strain indicator. A schematic of the strain measuring circuit is illustrated in Figure 9. Strain gages cemented on another specimen of the same material as that being tested were used as dummy gages. Additional strain gages cemented on a stainless steel plate were used to complete the measuring bridge network. In this manner, all switching from gage to gage was accomplished outside of the measuring bridge network. Therefore, the strain indicator detected only the imbalance of the measuring bridges due to strain in the gages on the test specimen, and changes in contact resistance due to switching were effectively bypassed. Furthermore, using a gaged specimen of the same material as a dummy reduced the possibility of obtaining false strain indications due to thermal fluctuations and consequent changes in length of the specimen. Switching was performed with a four-deck rotary switch.

The microyield stress of each tested specimen was calculated by plotting the average residual strain of the three gages versus stress. An appropriate vertical line was fitted to the data points obtained at low stress levels (i.e., below stresses at which significant residual

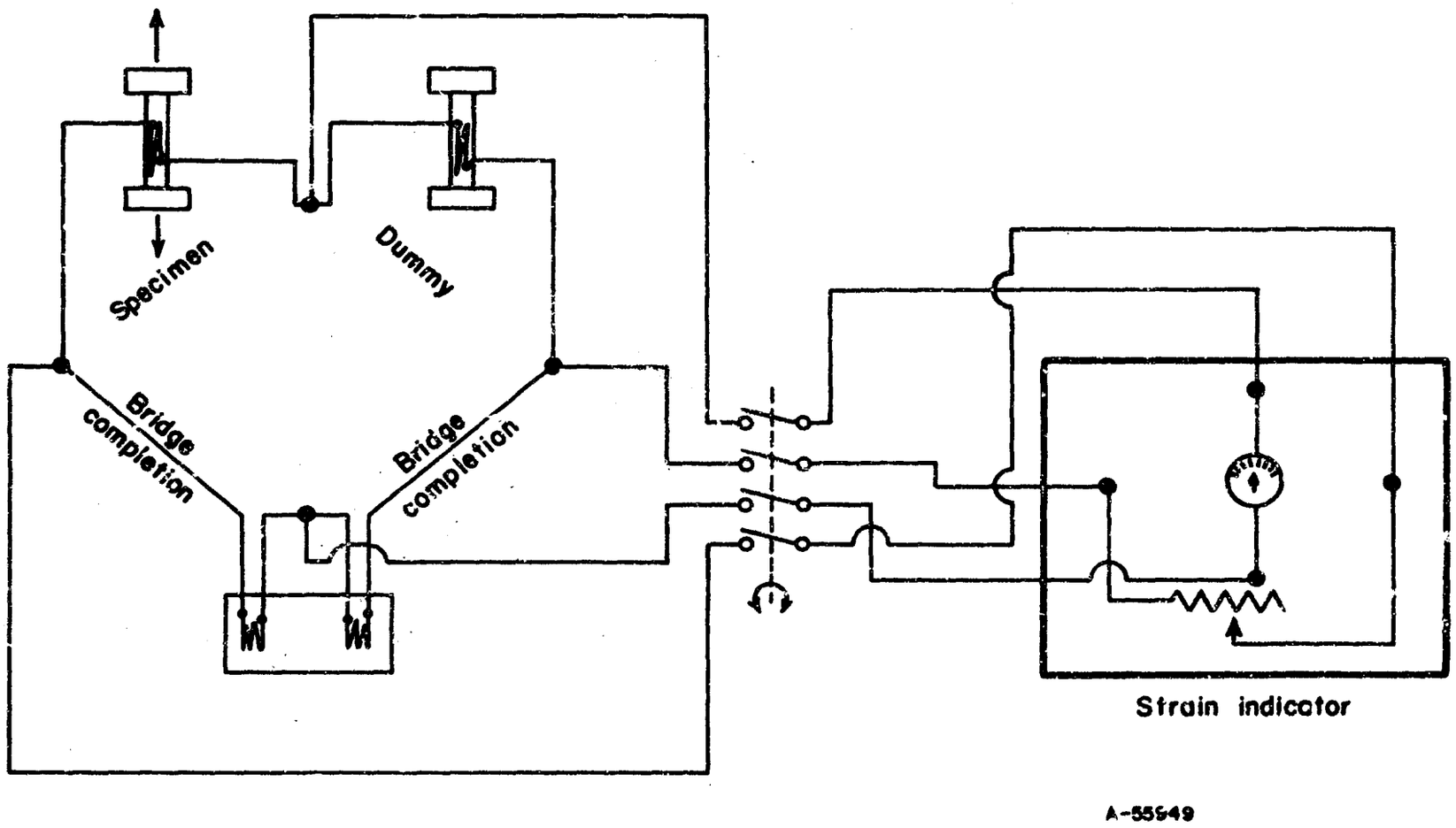

FIGURE 9. SCHEMATIC OF STRAIN-MEASURING CIRCUIT

strains were apparent). This line was generally displaced from the initial average zero strain indication of the gages by up to approximately 0.3 μin./in. The data points below the microyield stress were most often within ± 0.2 μin./in. of this reference line for zero strain. A second vertical line was then drawn offset from the reference line by a positive strain of 1 μin./in. The point at which this second line intersected a smooth curve drawn through the data points not falling on the reference line was taken as the microyield stress of the specimen.

Microcreep Limit. The procedures employed for microcreep limit testing were identical to those used for microyield stress testing with the exception that the stress was maintained on the specimens for up to 15 minutes.

Conventional Tensile Properties. The 0.2 percent offset yield stress, ultimate tensile strength, elongation, and reduction in area were determined by standard techniques and need not be elaborated upon here.

Dimensional Stability Testing

Machining Studies

Residual stresses introduced by machining are being determined by measuring the length of a machined specimen, chemically milling away the machined surface, and measuring the length a second time. The change in length upon chemical milling is a function of the average residual stress in the removed layer. This stress (σ) can be calculated by the equation,

$$\sigma = \frac{(d_F)^2 \, E \, \frac{L_F - L_o}{L_o}}{d_o^2 - d_F^2} \quad ,$$

where E is the modulus of elasticity, d_o is the initial diameter, d_F is the final diameter, L_o is the initial length, and L_F is the final length.

Specimen Preparation. Figure 10 illustrates the design of the specimen being used for the machining studies. They are prepared by the same procedures previously described for the mechanical-property specimen with the exception that the ends are lapped flat and parallel. The various machining procedures being evaluated will be performed on the large diameter, central portion of the specimens. The small-diameter ends of the specimens are used only to support the specimens in a specimen holder, and are not machined during the course of the study.

Etching Procedures. The etching procedures employed were similar to those used to prepare the tensile specimens for strain-gage application described in Table 4. However, greater control was exercised over the process to maintain roundness and taper to tolerances of less than 0.001 inch to facilitate subsequent machining operations. The electrochemical milling procedure was modified so that specimens of Ni-Span-C and 440 C stainless steel were revolved at 7 rpm between two copper strip cathodes. No major modifications were necessary for the chemical milling of A 356 cast aluminum and Ti-5Al-2.5Sn.

Instrumentation. An electromechanical gage block comparator is being used to measure the length of the specimens to a precision of 1 μin./in. This instrument compares the length of the specimens to the

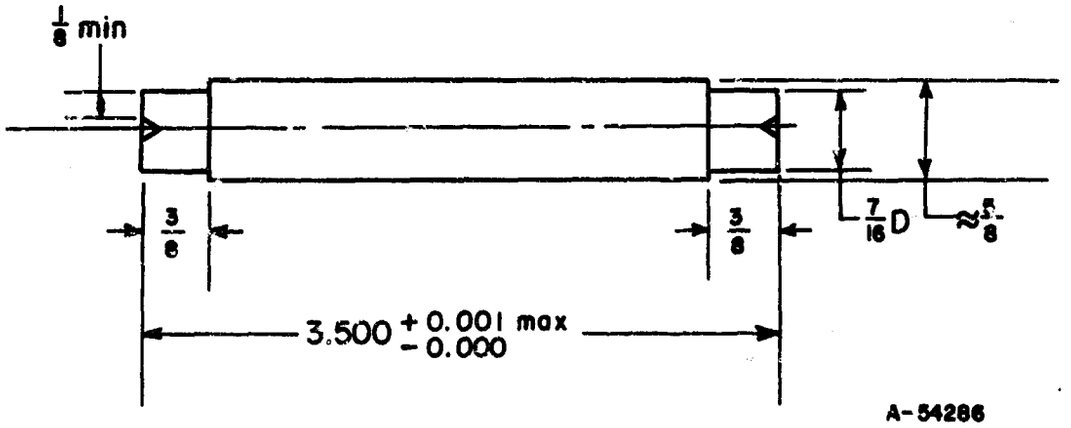

FIGURE 10. SPECIMEN FOR DIMENSIONAL-STABILITY STUDIES

length of a gage block of known length.

Figure 11 illustrates the test setup. The specimen is held vertically in a V-block, specimen holder. The back of the specimen holder is placed against the front surface of a gage block which in turn is held in position by a positioning fixture. The entire assembly rests on a base plate that is moved by a screw thread to sequentially pass the gage block and specimen between two measuring contacts. One contact is inert and serves only to position the second head that is coupled to an induction transformer. The movement of the second head, as the gage block is removed and the specimen is inserted, is electronically amplified and thus, indicates the difference in length between the gage block and the specimen. It is imperative that the contacts be brought back to the same point on the specimen to measure its length to the required precision. Angular alignment of the specimen is achieved with index marks on the V-block and specimen shoulders. Lateral positioning is fixed by the positioning fixture on the base plate, and travel of the base plate is indicated by a dial indicator that contacts the back surface of the gage block.

Considerable effort was devoted to developing necessary equipment and operator techniques to enable measurement of the specimens to the required precision. Specially ground, diamond contacts 1 inch in diameter were purchased to permit measuring the specimens without scratching or indenting the lapped ends. The specimens are placed on an aluminum soak-block at least one day before they are measured to bring them into thermal equilibrium. In addition, the specimens are allowed to sit before they are measured for at least 1 hour after

38155

FIGURE 11. PRECISION LENGTH MEASUREMENT TEST SETUP

they are fastened into the V-block and the assembly is placed on the base plate.

Effect of Load Cycles, Thermal Cycles, and Plastic Strain

The influence of load and thermal cycling, and plastic strain on dimensional stability will be determined by applying various mechanical and thermal treatments to specimens and determining their change in length over a period of time. The specimen design illustrated in Figure 1 for mechanical-property testing will be used. However, the ends will be lapped flat and parallel to facilitate making length measurements. Load cycles and plastic strain will be applied with a tensile testing machine. Length measurements will be made to a precision of 1 μin. using the same equipment and techniques described for the machining study.

MICROPLASTIC PROPERTIES

Microyield Stress Studies

Ni-Span-C

Microyield stress data for Ni-Span-C are illustrated in Figures 12, 13, and 14. The individual tests are in good agreement. An average microyield stress of 39 - 40 ksi is indicated. This is somewhat lower than the value of 57.5 reported by MIT.[1]

440 C Stainless Steel

Microyield stress data for 440 C stainless steel are presented in Figures 15, 16, and 17. The three separate tests are in excellent agreement. An average microyield stress of 69-70 ksi is indicated. A comparison of these data with those for Ni-Span-C reveals that not only is the microyield stress of 440 C stainless steel higher, but 440 C stainless steel also provides considerably more resistance to microplastic flow at stress levels above the microyield stress. For example, at a stress of 10 ksi above the microyield stress, Ni-Span-C shows a residual strain of 4-5 μin./in., whereas 440 C stainless steel exhibits a residual strain of only 2-3 μin./in. The microyield stress determined in this program is significantly lower than the value of 190.0 reported by MIT.[1]

A 356 Cast Aluminum

Figures 18 and 19 illustrate microyield stress data for A 356 cast aluminum. The variation in the indicated microyield stress

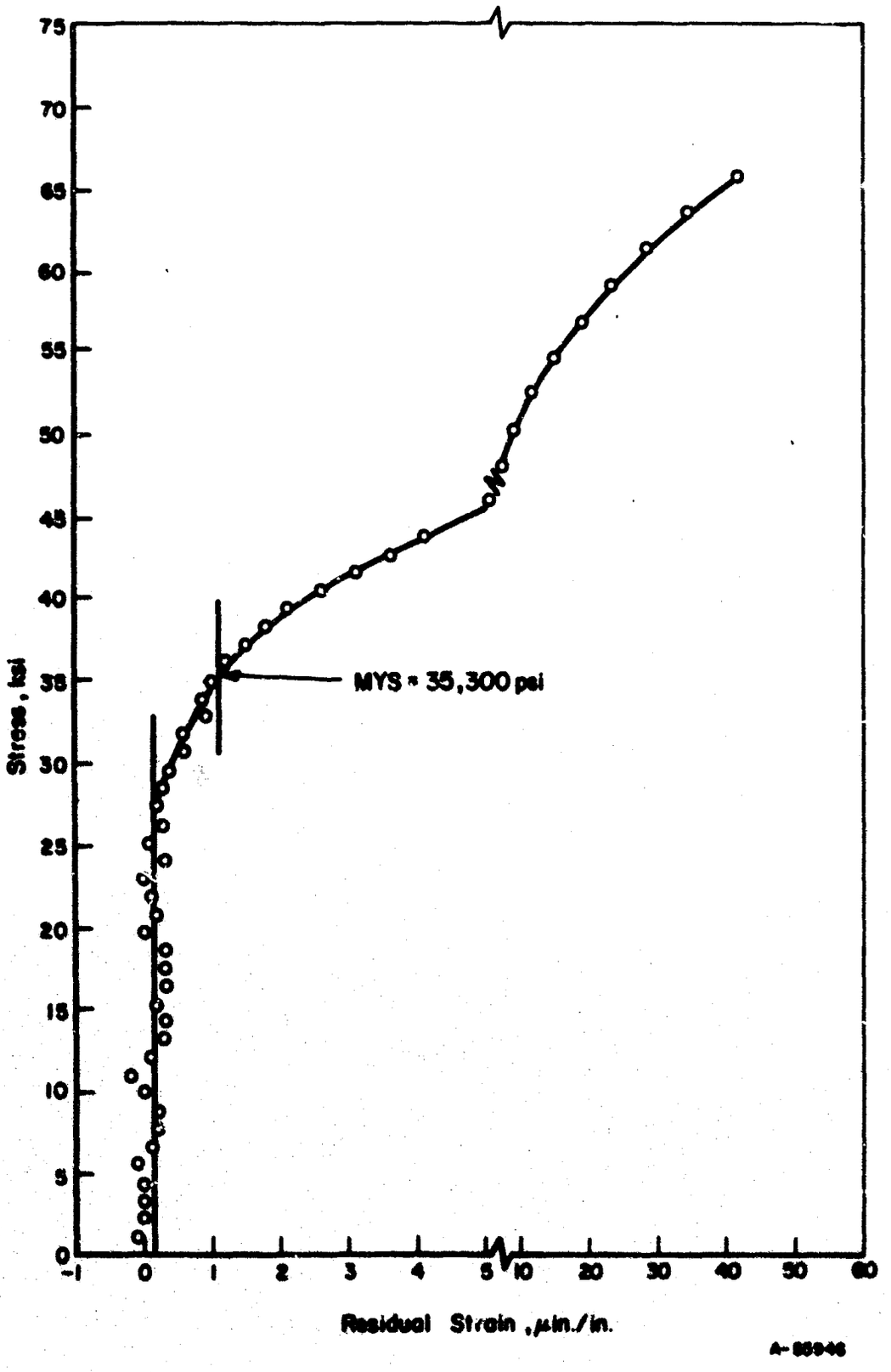

FIGURE 12. MICROYIELD STRESS OF Ni-SPAN-C SPECIMEN 5

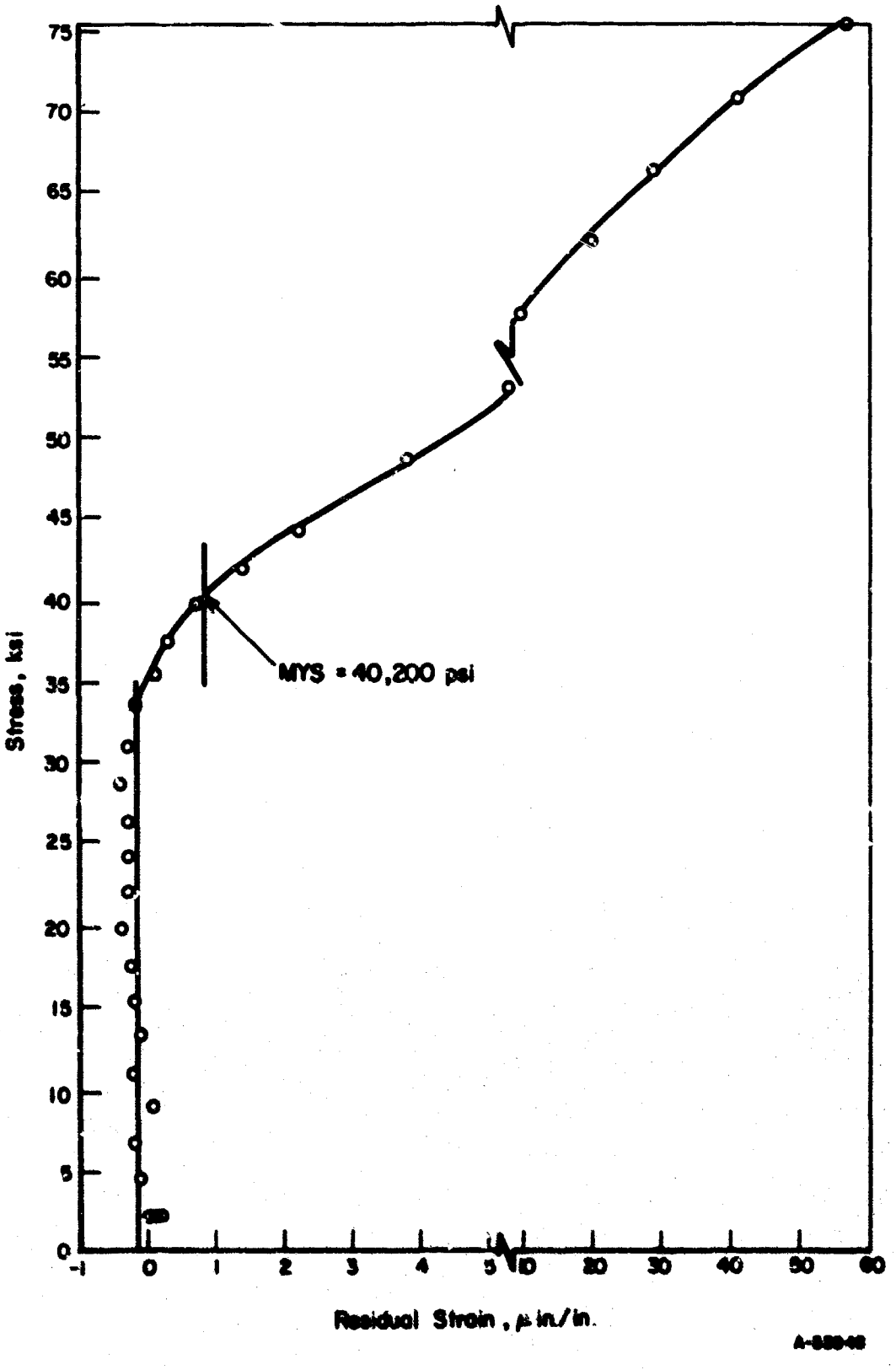

FIGURE 13. MICROYIELD STRESS OF Ni-SPAN-C SPECIMEN 6

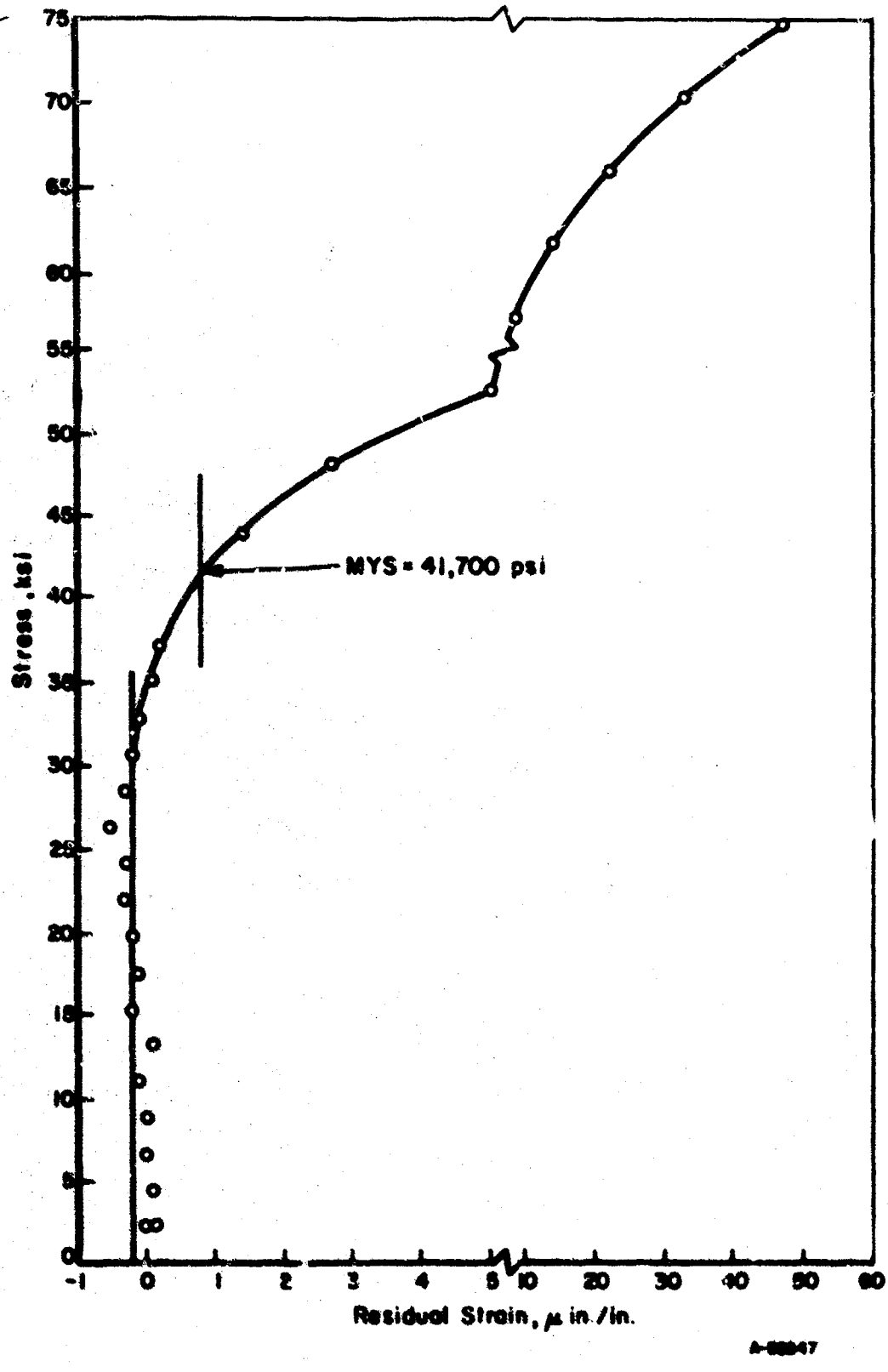

FIGURE 14. MICROYIELD STRESS OF Ni-SPAN-C SPECIMEN 16

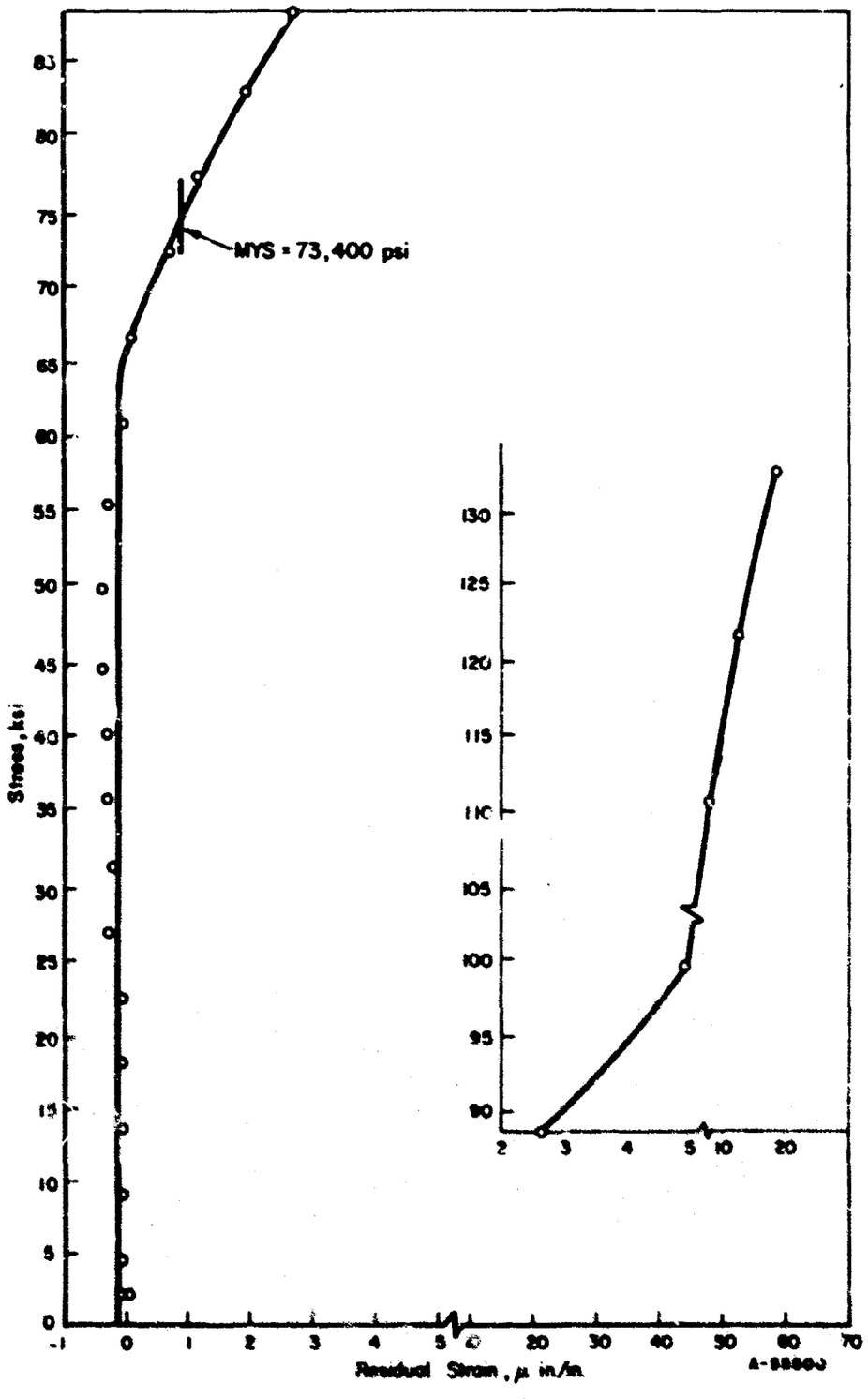

FIGURE 15. MICROYIELD STRESS OF 440 C STAINLESS STEEL SPECIMEN 9

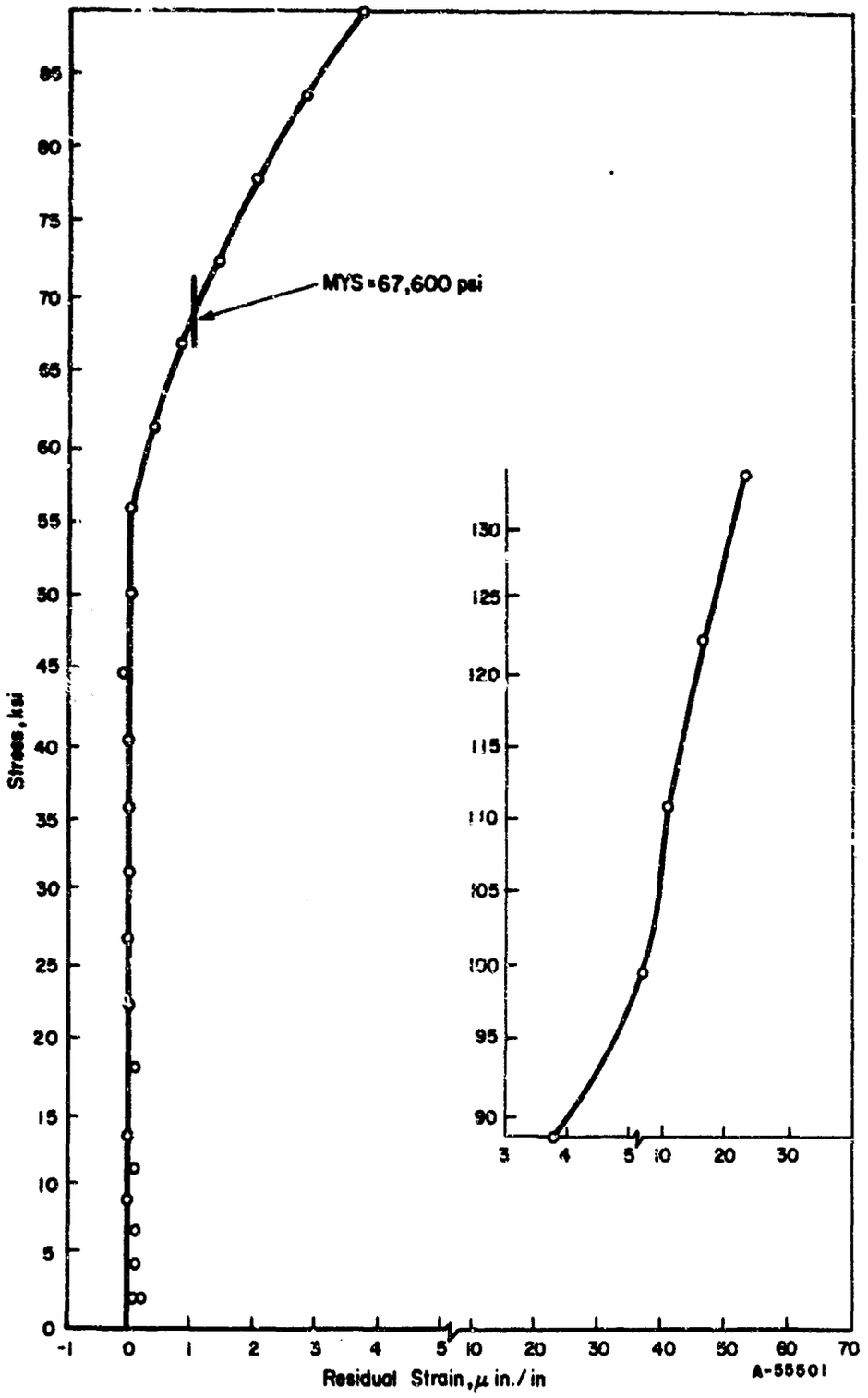

FIGURE 16. MICROYIELD STRESS OF 440 C STAINLESS STEEL SPECIMEN 7

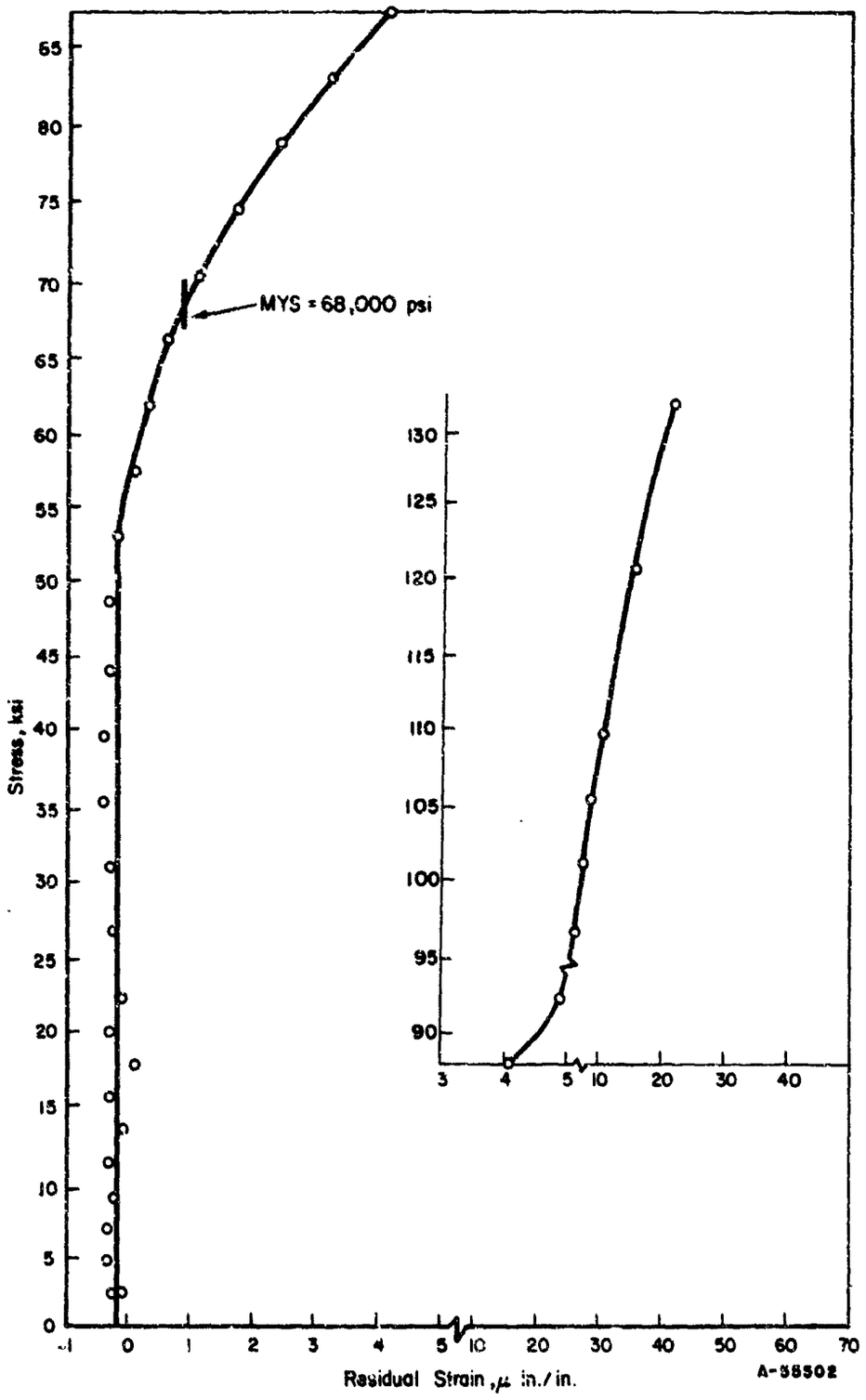

FIGURE 17. MICROYIELD STRESS OF 440 C STAINLESS STEEL SPECIMEN 4

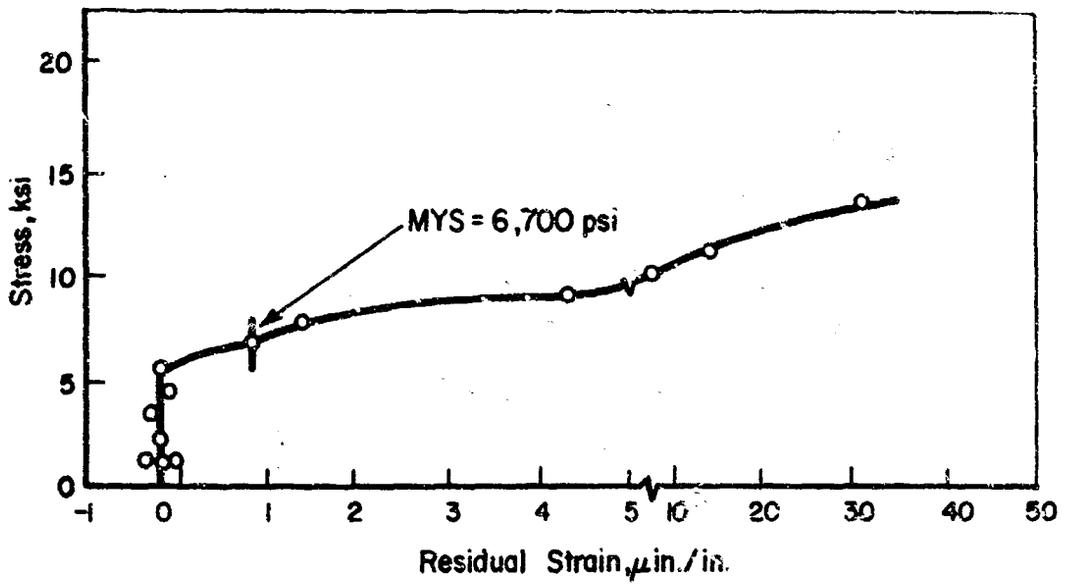

FIGURE 18. MICROYIELD STRESS OF A356 CAST ALUMINUM SPECIMEN 1

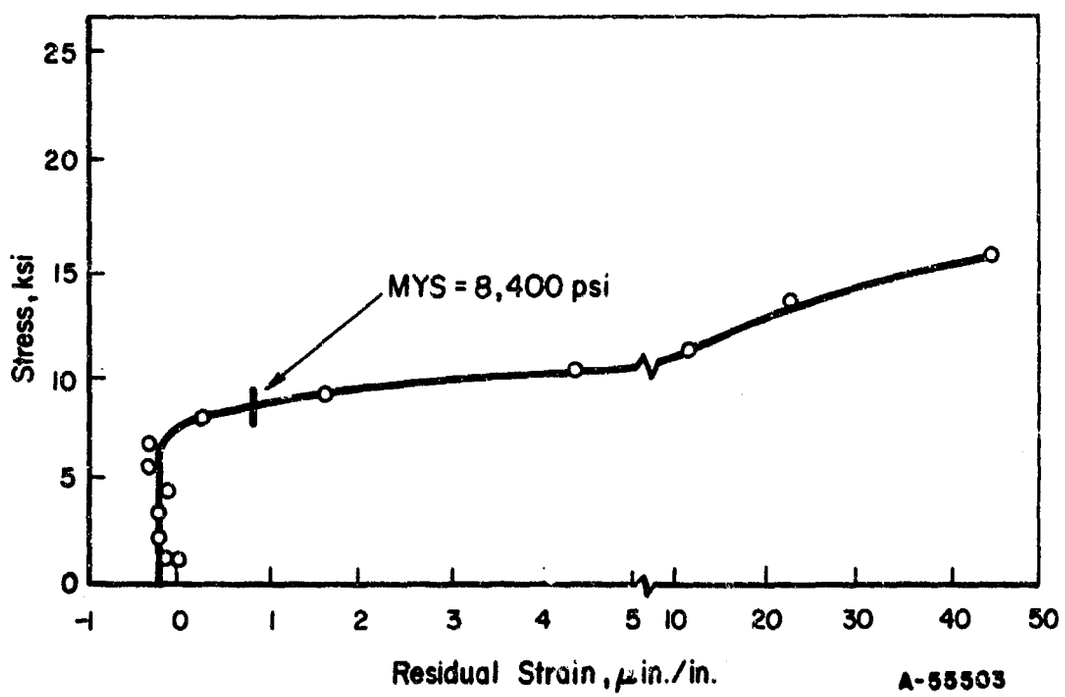

FIGURE 19. MICROYIELD STRESS OF A356 CAST ALUMINUM SPECIMEN 2

is somewhat greater than that obtained with Ni-Span-C and 440 C stainless steel, but this is considered to be normal for cast aluminum. An average microyield stress of approximately 7.5 ksi is indicated. This is slightly lower than the value of 12.0 ksi reported by MIT.[1] Not only is this microyield stress much lower than that of Ni-Span-C and 440 C stainless steel, but the resistance to microplastic flow once the microyield stress has been exceeded is far less as well. At a stress of only 5 ksi greater than the microyield stress, a residual strain of 20-30 μin./in. is obtained.

Ti-5Al-2.5Sn

Efforts to obtain a satisfactory microyield stress with Ti-5Al-2.5Sn have been unsuccessful to date. For titanium alloys, the combination of high strength and low modulus of elasticity results in the gages being strained upon loading beyond their ability to respond elastically in the load-unload microyield stress test. As a consequence, negative residual strains were indicated after unloading from stress levels above approximately 20,000 psi. It is expected that the capacitor strain gage described in a following section of this report will be used to measure microstrains in Ti-5Al-2.5Sn as soon as improved attachment techniques are perfected.

Beryllium

Microyield stress tests will be conducted as soon as the material is received and specimens are prepared.

Aluminum Oxide

Two specimens of aluminum oxide have been tested. Brittle failure occurred in both specimens at the fillet between the loading shoulders at stresses of 10.5 and 11.7 ksi, and no evidence of micro-plastic flow was detected. The shoulders of two additional specimens were coated with wax to more uniformly distribute the load, but the same difficulty was encountered.

Brittle ceramics have been successfully tested by cementing metallic loading shoulders on cylindrical rods of the ceramic. Additional material has been ordered, and efforts will be made to obtain a meaningful microyield stress using this type of specimen.

Microcreep Limit Studies

Microcreep limit data for 440 C stainless steel held at load for 5 and 15 minutes are illustrated in Figure 20. Only slightly greater residual strains were observed when the specimens were held at load, as compared with strains measured in the microyield stress test in which the load was released immediately upon attainment of the desired stress. There was no measurable difference between the residual strains after holding for 5 and 15 minutes at load.

Figure 21 illustrates microcreep limit data for Ni-Span-C. Similar to 440 C stainless steel, holding at load for 15 minutes did not result in significantly greater residual strains than were obtained in the microyield stress test.

It appears that microcreep limit tests, as they have been conducted this far, are of marginal value. Conventional creep tests

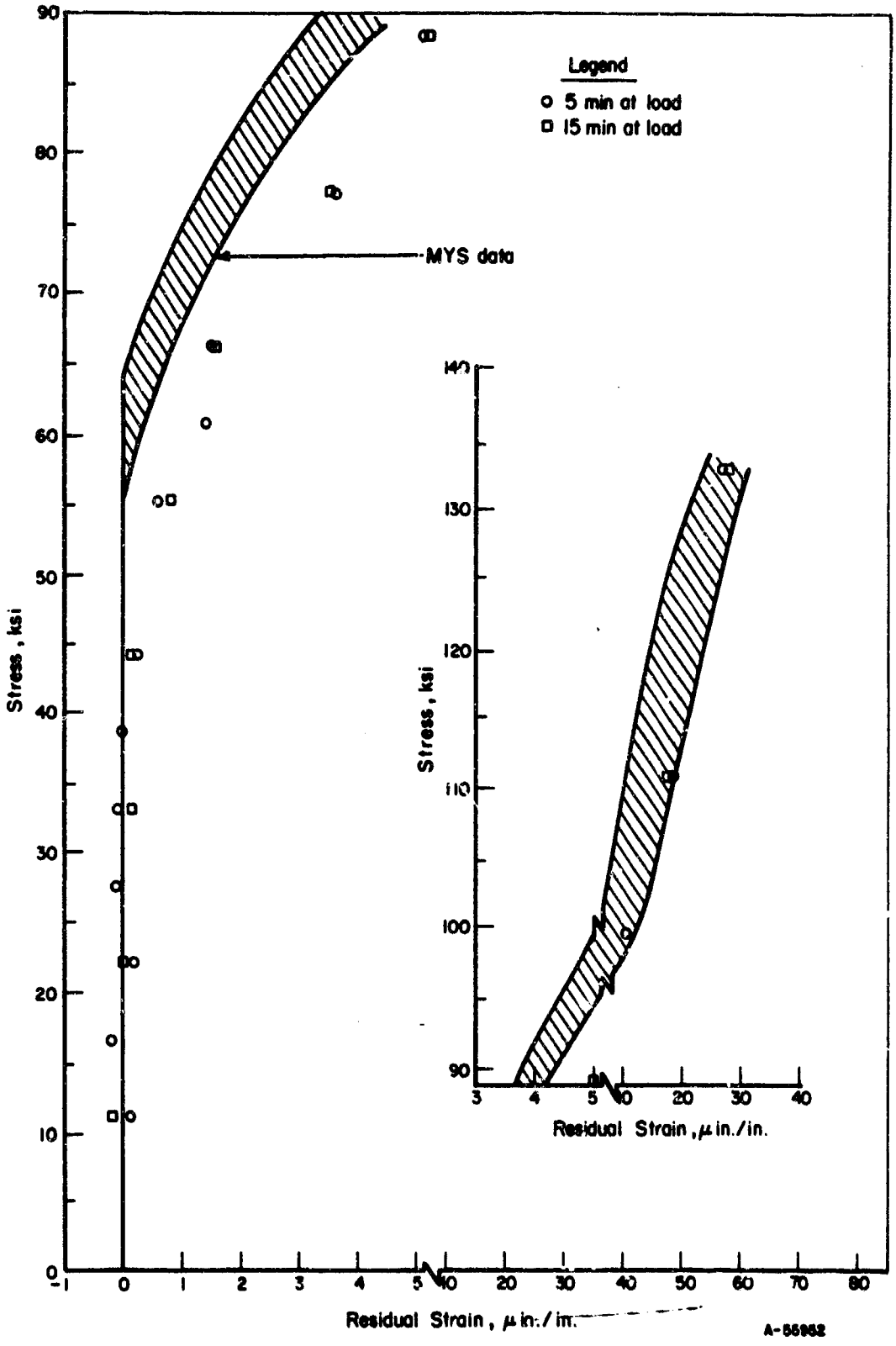

FIGURE 20. MICROCREEP LIMIT DATA FOR 440 STAINLESS STEEL

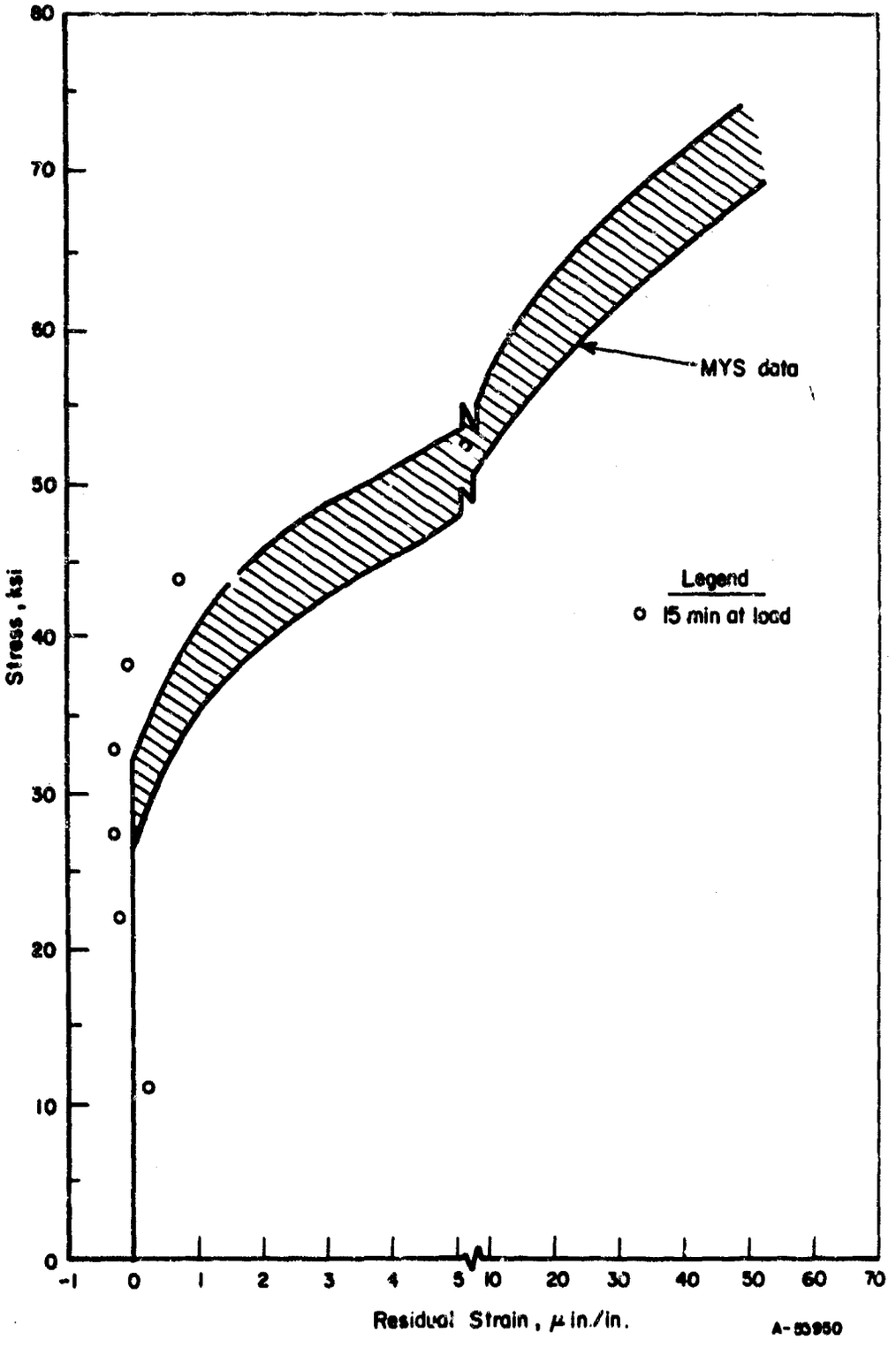

FIGURE 21. MICROCREEP LIMIT DATA FOR Ni-SPAN-C

for longer periods on specimens dead-weight loaded to stress levels below the microyield stress would appear to yield more useful data; therefore, future efforts will be in this direction.

Mechanisms of Microplastic Deformation

Initial observations concerning the basic mechanisms of microplastic deformation have been made by examining in an electron microscope thin foil sections of strained and unstrained portions of tested microyield strength specimens. It should be remembered that only a relatively few foils have been examined and the following discussion is, therefore, somewhat speculative.

Ni-Span-C

Unstrained foils of Ni-Span-C generally displayed a near absence of dislocations as shown in Figure 22a. Second phase particles were seen in the grain boundaries. Dislocations present were not distinctly associated with any other microstructural feature as can be seen in Figure 22b. Observations on foils taken from microstrained material suggest that microstrain is the result of dislocation generation or movement away from microstructural stress raisers under an applied load. Figure 23 illustrates dislocations emanating from second phase particles in grain boundaries, the interrection of a twin and a grain boundary, and a jog in a grain boundary. Second phase particles in grain boundaries appeared to be prime locations for the nucleation of microplastic flow. This is in general agreement with the work of Davies and Ku[2] who studied dislocation generation in Fe-3-1/4 Si by etch-pit techniques.

15,000X a. E2245d

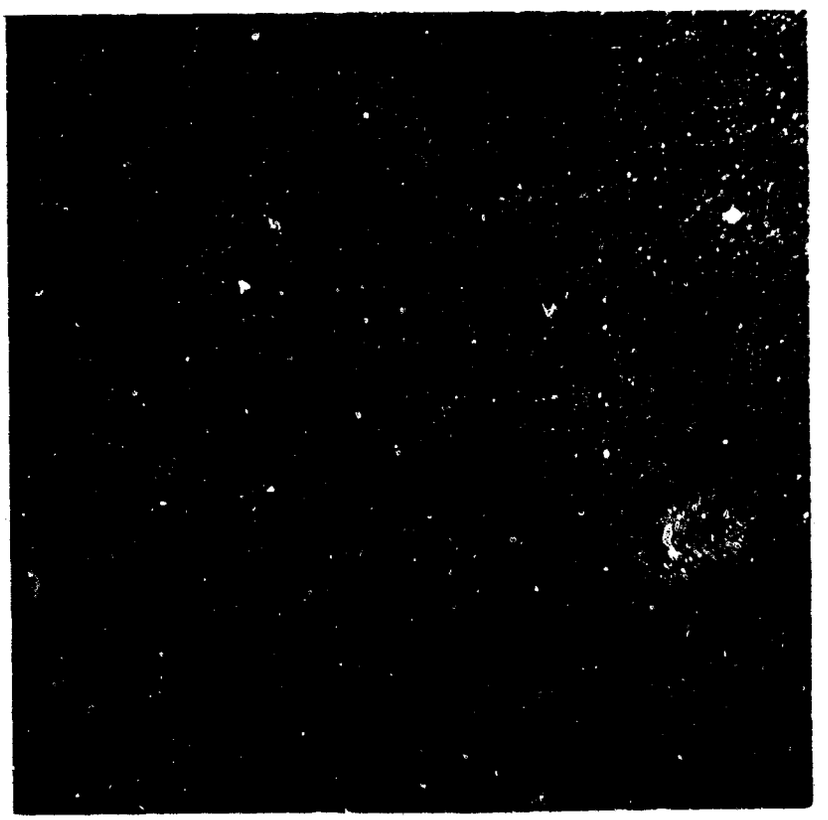

15,000X b. E2246c

FIGURE 22. UNSTRAINED NI-SPAN C

15,000X a. Grain-Boundary Second Phase E2244d

15,000X b. "Jog" in Grain Boundary E2243e

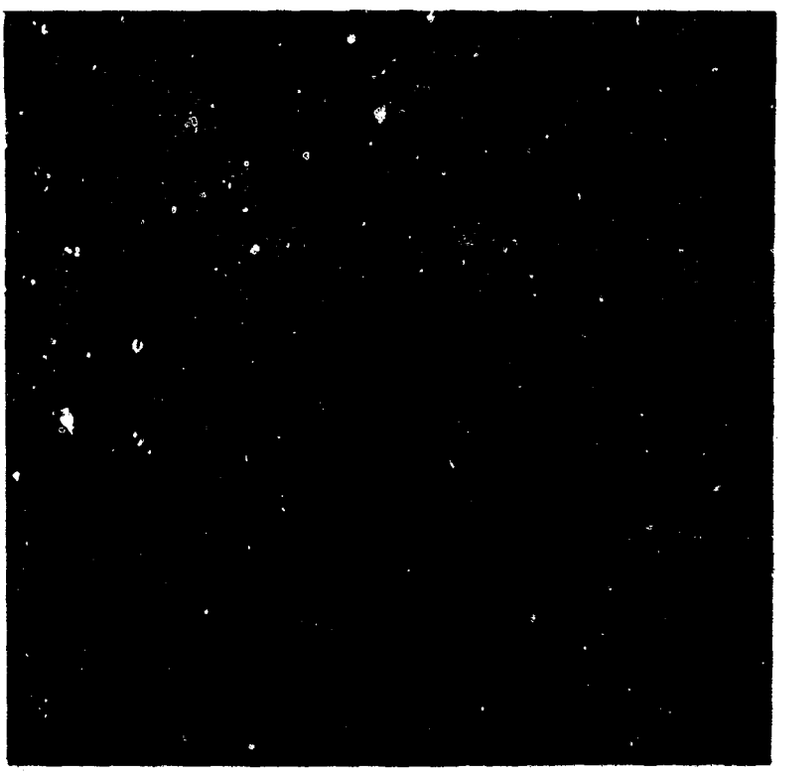

80,000X c. Intersection of Twin and Grain Boundary E2243a

FIGURE 23. MICROSTRAINED (4[illegible] μin./in.) NI-SPAN C

It is also of interest that little evidence of dislocation interaction with other dislocations or defects was detected.

A 356 Cast Aluminum

Evidence of microplastic flow in A 356 cast aluminum is somewhat more subtle than for Ni-Span-C. Foils of unstrained material revealed rod-like precipitate particles (probably Mg_2Si) in the grain interiors, as shown in Figure 24. The relatively diffuse contrast around the particles indicates a distortion of the matrix lattice due to the presence of the particles. Foils of strained material generally exhibited a somewhat sharper contrast around the particles as illustrated in Figure 25a, b, and c. This sharper contrast suggests that microstrain could be a result of a transformation of lattice distortions around the particles into interfacial dislocations under an applied load. Many of the dislocations appeared to form spirals or loops around the particles. In some instances, as shown in Figure 25d and e, some dislocations appeared to move away from the original particles and several of the dislocations connected with other particles.

Tangled knots of dislocations were on occasion observed around the precipitate particles as illustrated in Figure 26. However, these knots were noticed in both strained and unstrained foils. Therefore, they were probably either in the material before testing or were introduced during foil preparation, and are not the result of microplastic deformation.

44,000X a. EH421

44,000X b. EH431

44,000X c. EH441

FIGURE 24. UNSTRAINED A356 CAST ALUMINUM

42,000X a. EH446

42,000X b. EH451

42,000X c. EH4[illegible]

FIGURE 25. MICROSTRAINED (40 μin./in.) A356 CAST ALUMINUM

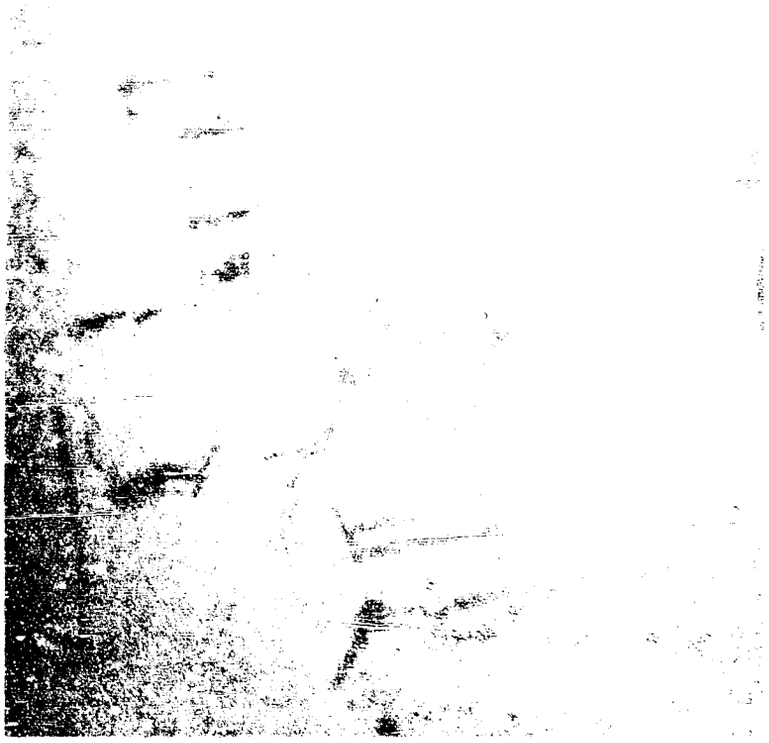

42,000X d. EH453

42,000X e. EH447

FIGURE 25. (CONTINUED)

44,000X EH437

FIGURE 26. KNOTS OF TANGLED DISLOCATIONS IN A356 CAST ALUMINUM

440 C Stainless Steel

Thin foils prepared from unstrained 440 C stainless steel revealed carbide particles in a martensitic matrix with a very high dislocation density as shown in Figure 27. This high dislocation density is characteristic of martensite and prevented any meaningful interpretation of the structure of foils taken from strained material with regard to microplastic deformation. However, these foils are still useful in interpreting the micromechanical properties of 440 C stainless steel. The high dislocation density in 440 C stainless steel, as compared to the very low dislocation density of Ni-Span-C, may account for the higher microyield stress and greater resistance to continued microplastic deformation of 440 C stainless steel.

Metallographic specimens of unstrained and microstrained Ni-Span-C and A 356 cast aluminum are being prepared for dislocation etch pit examination. If successful these specimens should give an indication of dislocation multiplication due to microstraining, and the dislocation patterns can be compared to what has been postulated from the examination of the thin foils.

Microstrain Hardening and Recovery of Microstrain

Several tests were conducted in which 440 C stainless steel microyield test specimens were reloaded both immediately and with a 24-hour delay after initial determination of the microyield stress. An example of such a test is illustrated in Figure 28. Microyielding occurred in reloaded specimens at significantly higher stress than the

15,000X E2249d

FIGURE 27. UNSTRAINED 440C STAINLESS STEEL

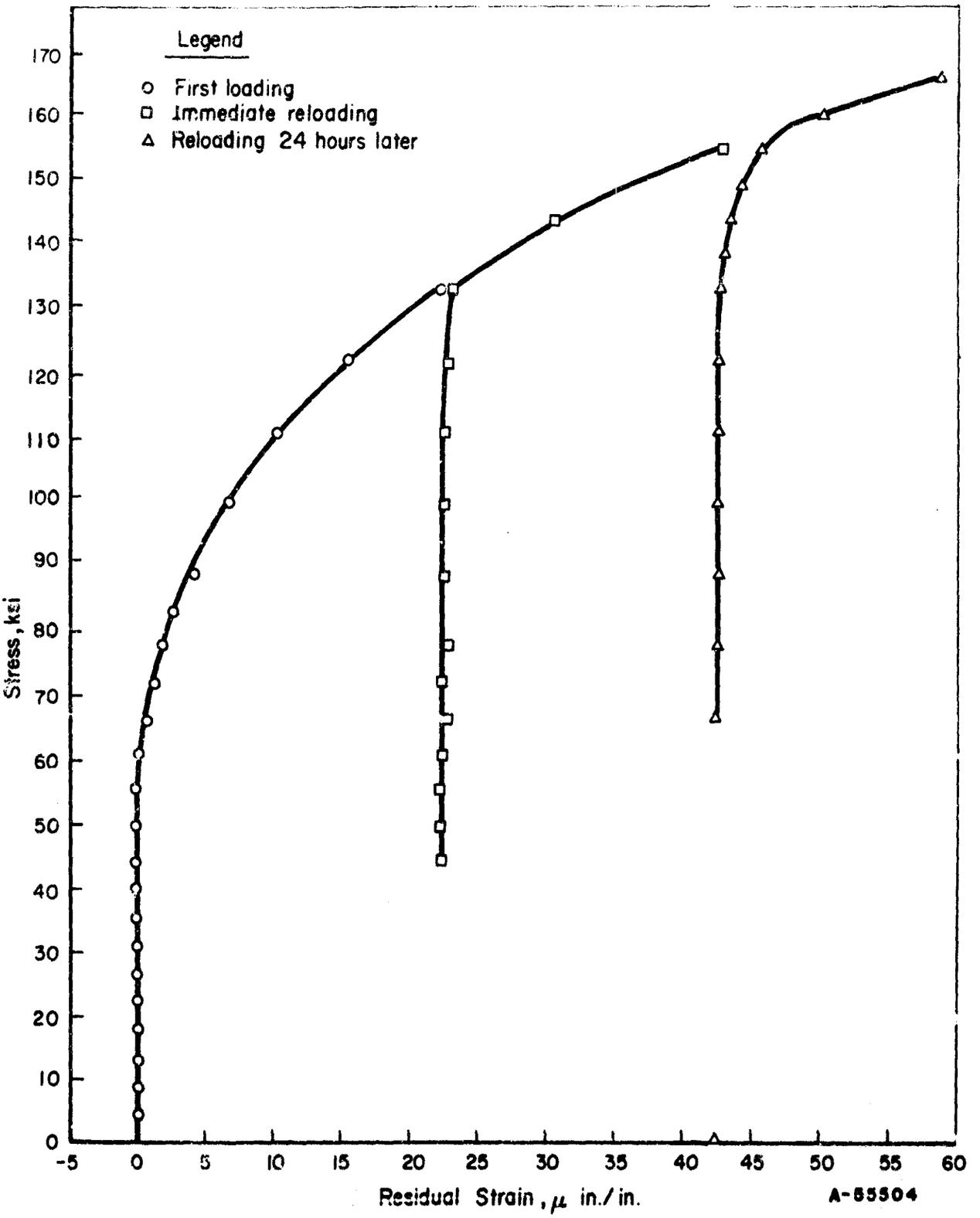

FIGURE 28. RECOVERY OF MICROSTRAIN IN 440 C STAINLESS STEEL SPECIMEN 7

initial microyield stress indicating "microstrain hardening". However, microyielding was detected at somewhat lower stresses than the previous maximum load suggesting some recovery of microstrain. Once appreciable microyielding occurred in reloaded specimens, the material followed the same stress-residual strain trace very closely.

Figure 29 summarizes the microstrain recovery characteristics of 440 C stainless steel. The extent of recovery can be viewed in two ways. First, the microyield stress of a reloaded sample was observed to occur at a stress lower than that to which the specimen had been previously subjected. Second, the specimen showed additional strain on reloading to the previous maximum load.

Recovery is a sensitive function of delay time to retest and previous microstrain in the material. Almost no recovery was evident upon immediate retest of a specimen with a residual strain of approximately 20 μin./in. Appreciably more recovery was noted upon immediate retest of a specimen with a residual strain of approximately 40 μin./in. In the latter case a microyield stress was observed about 6,000 psi below the previous maximum stress, and an additional 2 μin./in. residual strain was retested after a 24-hour delay. A microyield stress at approximately 9,000 psi below the previous maximum stress and an additional 3 μin./in. residual strain at maximum load were observed upon retesting a specimen with approximately 40 μin./in. residual strain after a 24-hour delay.

The data illustrated in Figure 28 also suggest the possibility of increasing the microyield stress by microstraining similar to the way in which cold working increases conventional mechanical properties. However, the effect of microstrain on dimensional stability must be taken

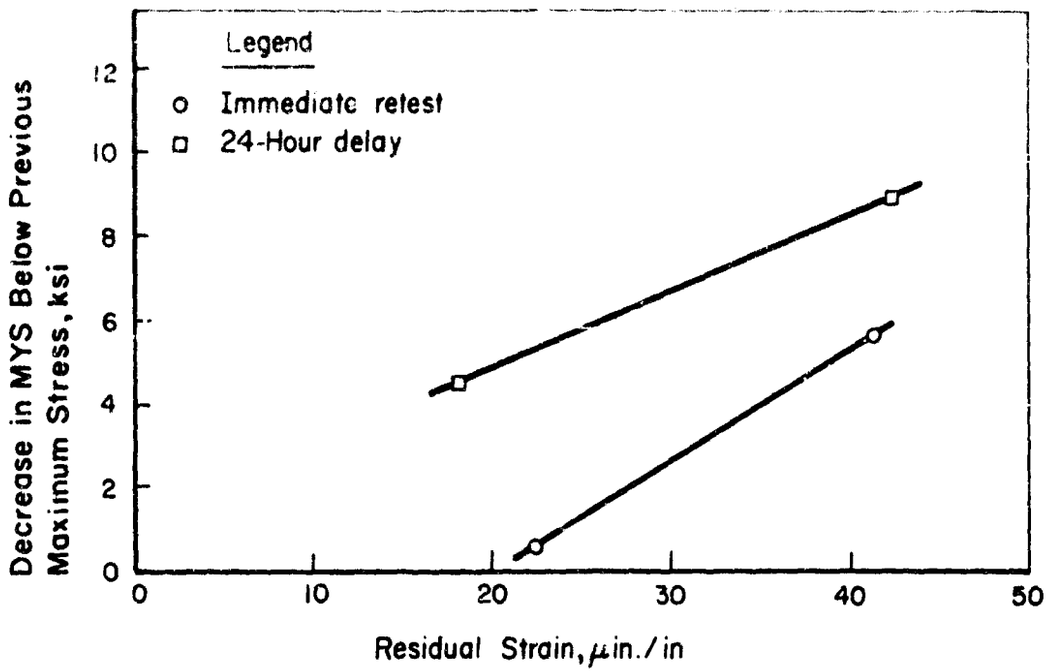

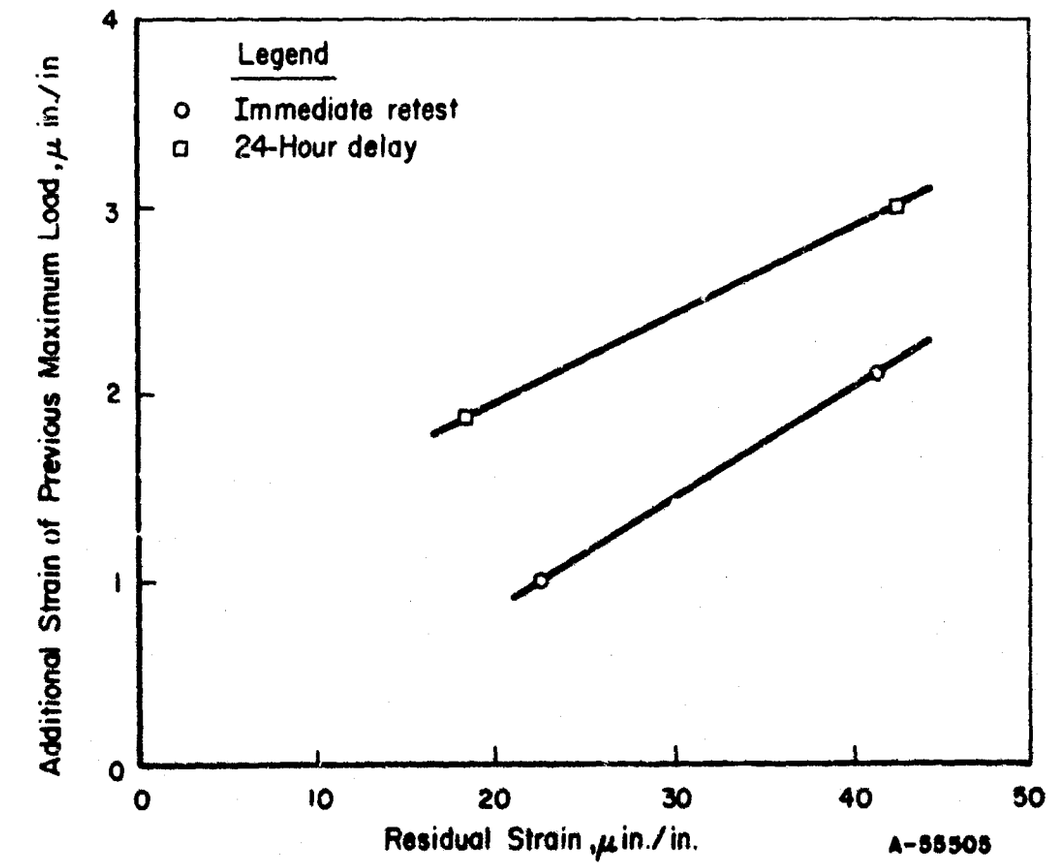

FIGURE 29. RECOVERY OF MICROSTRAINED 440 C STAINLESS STEEL

into account. Microstrains may accelerate dimensional changes and thus preclude their use to improve micromechanical properties. The influence of plastic strain (including microstrain) on dimensional stability will be studied in a subsequent phase of this research program.

A similar series of experiments is being conducted for Ni-Span-C.

Conventional Tensile Properties

The conventional mechanical properties of Ni-Span-C, 440 C stainless steel, and A 356 cast aluminum are given in Table V. Figure 30 compares the conventional yield stress with the microyield stress of these three alloys.

TABLE V. CONVENTIONAL MECHANICAL PROPERTIES

Material	0.2% Offset Yield Stress, ksi	Ultimate Tensile Strength, ksi	Elongation, percent	Reduction in Area, percent
Ni-Span-C	106.7	175.5	12	49
	102.1	173.6	12	54
440 C	(a)	255	0	0
	(a)	214	0	0
A 356	22.2	31.2	2	2
	21.2	31.1	3	2.5

(a) Fracture before yielding

It appears that alloys with higher conventional yield stresses also have higher microyield stresses. However, the microyield stress tended to be a smaller fraction of the conventional yield stress the higher the conventional yield stress. This suggests that optimum alloy

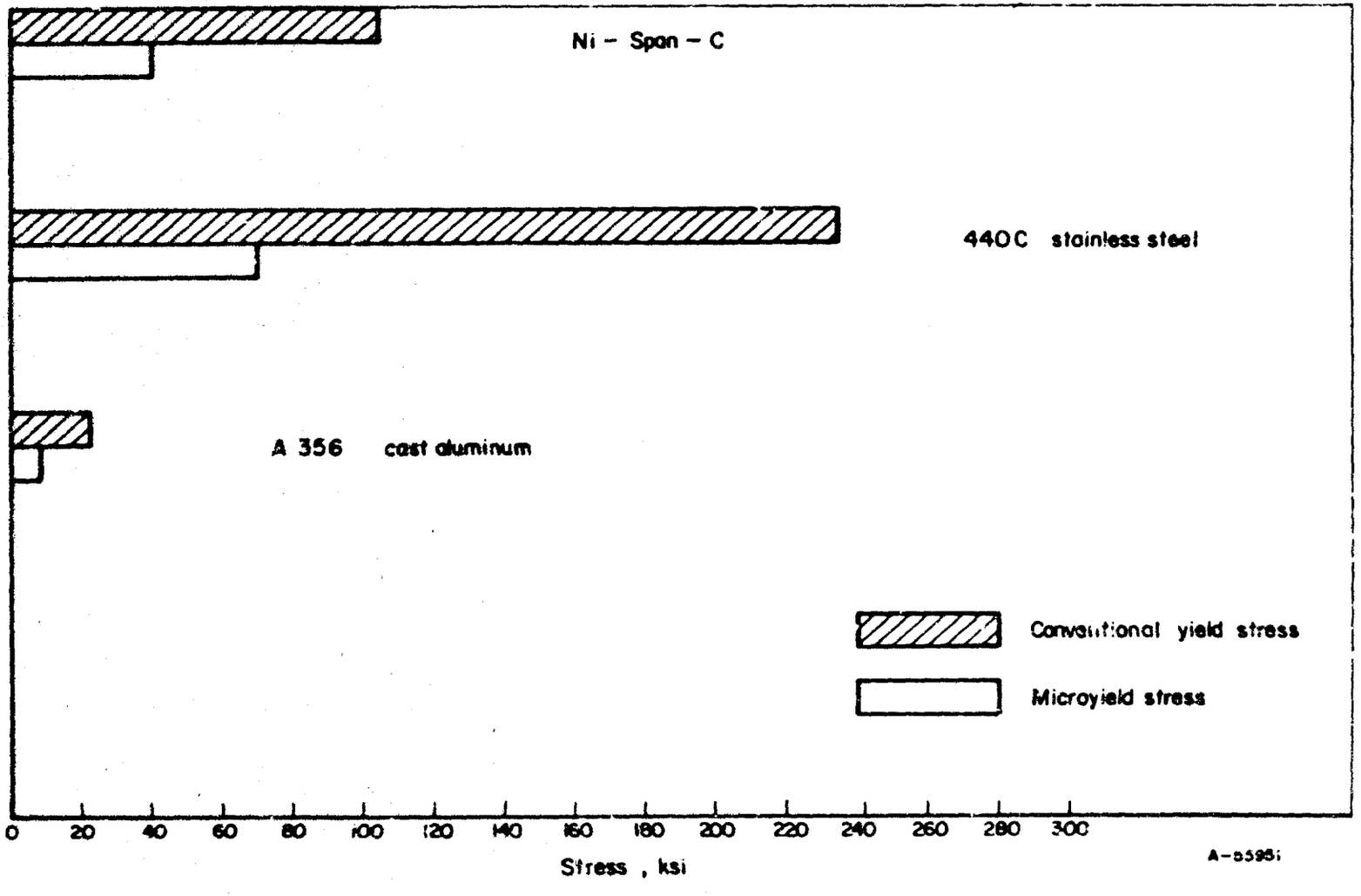

FIGURE 30. COMPARISON OF CONVENTIONAL YIELD STRESS AND MICROYIELD STRESS

contents and processing procedures for high micromechanical properties may be quite different than those commonly employed for high conventional mechanical properties.

CAPACITOR STRAIN GAGE

A capacitor strain gage potentially offers a number of advantages as a strain measuring system. It should have high sensitivity, lower cost than electrical resistance strain gages, no dependence upon adhesives, and the capability of measuring larger strains than electrical resistance gages. It should also be particularly useful for determining the micromechanical properties of high strength-low modulus materials like titanium for which electrical-resistance strain gages are unsuitable.

Figure 31 illustrates a prototype capacitor strain gage designed to evaluate the separation of capacitor plates as a technique for the measurement of strains of 1 μin./in. or less. Initial experiments were conducted by attaching the gage elements to a length of annealed drill rod using cupped set screws. A variable capacitor was placed in series with the gage to reduce the effective plate area and obtain the desired sensitivity. A Wayne-Kerr electronic micrometer was used as a readout device. Strain indications of the gage were compared to those of two electrical resistance strain gages applied to the same length of rod.

Apparent sensitivity of the capacitor gage was at least as good as the electrical resistance strain gages. The major problems encountered were deviation from linearity with elastic strains above approximately 20 μin./in., failure to track upon unloading, and inability to consistently indicate zero residual strain at a nominal reference load after applying stresses of less than 2.0 ksi. It was felt that all of these problems were attributable to slippage of the gage on the specimen, and were not inherent shortcomings of the gage itself.

1. Base clamp
2. Lower plate
3. Shield
4. Top clamp (Lucite)
5. Lucite insulation
6. Set-screw holes
7. Upper plate

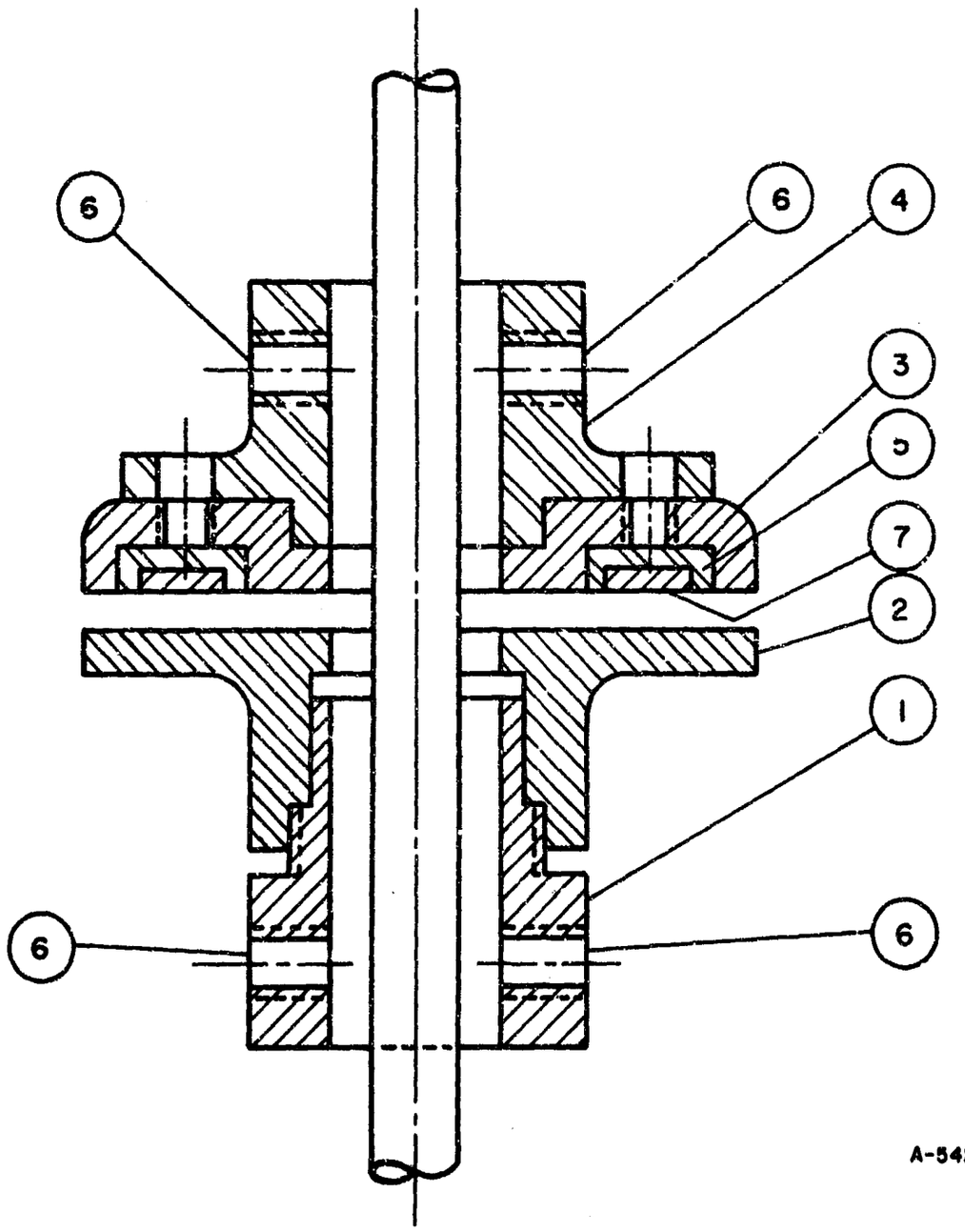

FIGURE 31. PROTOTYPE CAPACITANCE STRAIN GAGE

Attempts were made to eliminate slippage of the gage elements by using pointed and spring loaded, plunger set screws, but no significant improvement was noted. A specimen providing a shoulder for attaching the gage elements was then prepared. It was reasoned that the shoulders should undergo much less strain than the test section when the specimen is loaded, and thereby provide a more stable foundation for attachment of the gage. Tests demonstrated that this technique reduced slippage, but not sufficiently to make the gage useful for reliable microstrain measurements.

The design of the gage is currently being modified so that the elements can be supported by flanges on the specimen perpendicular to the loading axis. In this manner, the gage will rest upon an area of the specimen that is not strained when the specimen is loaded and unloaded, but the gage elements will still separate in direct relation to strain in the specimen.

DIMENSIONAL STABILITY

Much of the effort on this phase of the research was devoted to developing the necessary equipment and operator techniques required to measure the length of specimens of engineering alloys that are not as ideally suited to precision measurement as standard gage block materials. Procedures have been developed whereby length measurements can be made to a precision of 1 μin. Up to this time, these procedures have been employed primarily in the evaluation of the principal sources of residual stresses, since these stresses are believed to be the predominant cause of dimensional instability.

Machining Residual Stress Studies

Successive layers were etched off of Ni-Span-C and 440 C stainless steel specimens machined by common machine shop practice. The change in length data, along with the computed residual stresses corresponding to the changes in length, are illustrated in Figures 32 and 33. The residual stresses, to a depth of 4 or 5 mils below the surface, are probably introduced by the combined effects of machining and heat treating. At depths greater than 5 mils, the residual stresses are most likely attributable to heat treating alone. Thus far, a maximum residual stress of 15 ksi in compression in Ni-Span-C and a maximum residual stress of 8 ksi in tension in 440 C stainless steel have been found. These experiments are being continued to establish the residual stress contour in each material to a depth of 30-40 mils. Similar data will be obtained for A 356 cast aluminum, Ti-5Al-2.5Sn, and beryllium. This information will then be used as base line data to

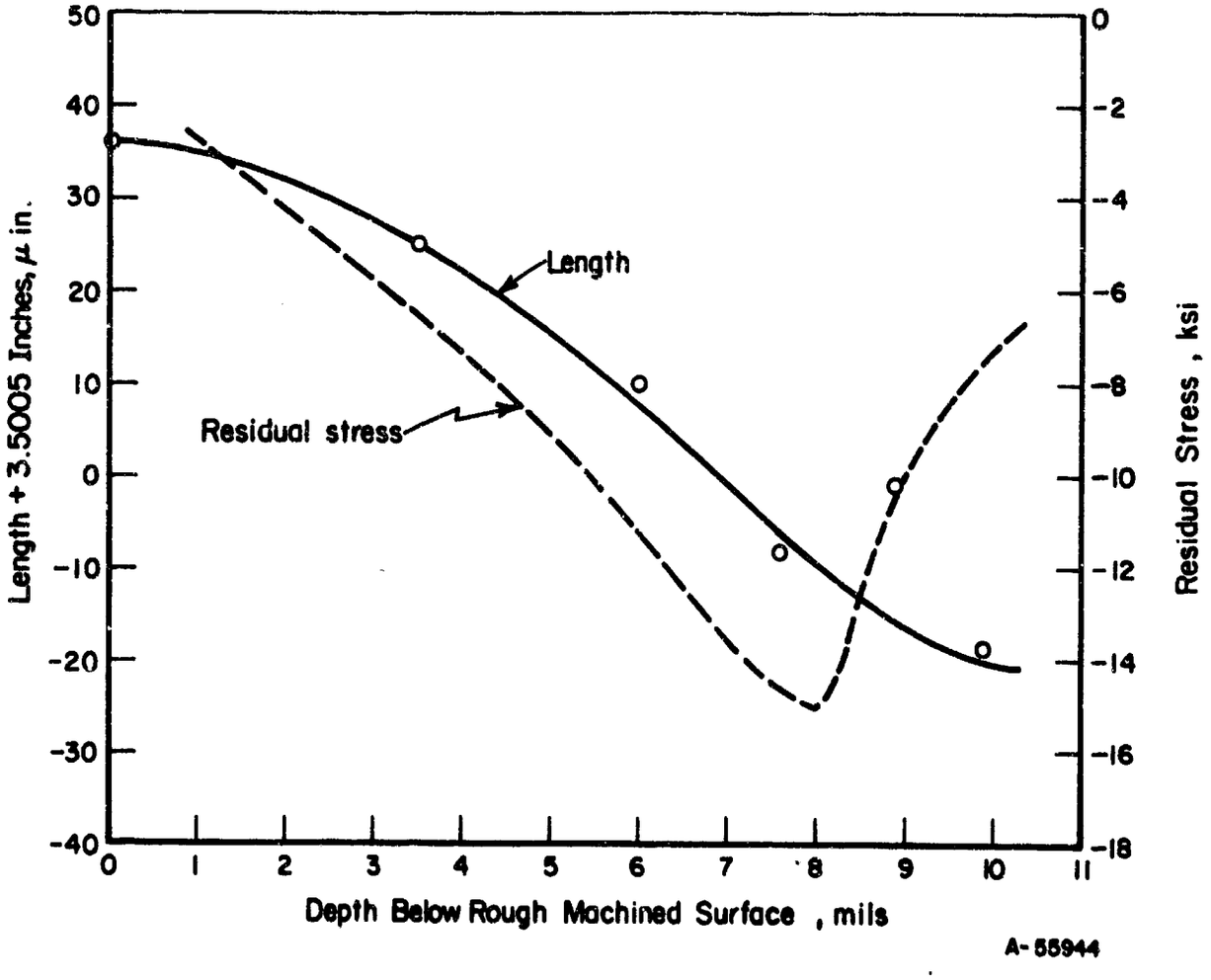

FIGURE 32. RESIDUAL STRESS CONTOUR IN ROUGH MACHINED Ni-SPAN-C SPECIMEN 11

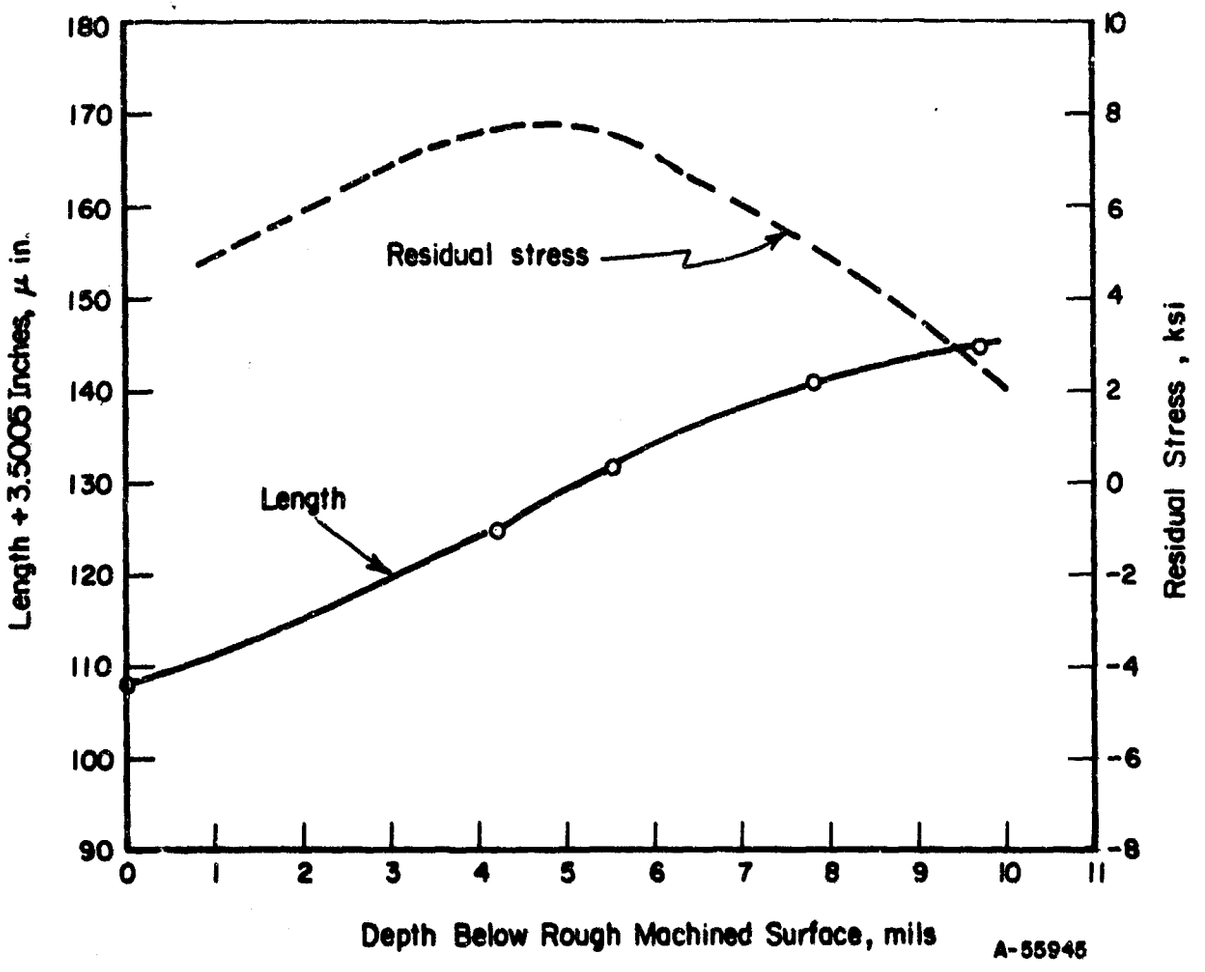

FIGURE 33. RESIDUAL STRESS CONTOUR IN ROUGH MACHINED 440 C STAINLESS STEEL SPECIMEN 11

assess the magnitude of the residual stresses introduced by various machining operations.

Specimens will be conditioned for the machining studies by etching 5 mils off the surface to remove any material affected by rough machining. Initially, the residual stresses introduced by one-pass machining cuts will be determined. Lathe cuts of 8, 5, 3, and 1 mil will be investigated for A 356 cast aluminum, Ni-Span-C, Ti-5Al-2.5Sn, and beryllium. Grinding cuts of 5, 3, and 1 mil will be evaluated for the harder 440 C stainless steel. These data will then be used to set up various sequences of cuts amenable to a final machining operation. An optimum final machining sequence will be selected for each material. Ultimately, other machining parameters such as rpm, tool feed, lathe turning vs. grinding, and lapping will be examined.

Effects of Plastic Strain

Plastic strains of 20-40 μin./in., 0.01 in./in., and 0.1 in./in. will be applied to tensile specimens with lapped ends. Length measurements will be made for periods of up to 6 months, and the change in length of strained material will be compared to that of unstrained specimens.

Thermal Cycling

The effects on dimensional stability of cycling between temperatures of 200 and -100 F will be examined. Changes in length of cycled specimens will be compared to uncycled control samples over a period of up to 6 months.

Load Cycling

The effects on dimensional stability of repeatedly loading to stresses less than the microyield stress will be studied.

Dimensional Stability of Zyttrite

The ends of the two zyttrite specimens supplied by the Air Force have been gound flat and parallel, and special specimen holders have been prepared. These specimens will be periodically measured over a period of at least 6 months to establish their dimensional stability characteristics.

CONCLUSIONS

Because the research program is only at its midpoint, it would be premature to attempt a lengthy discussion of the results. However, some conclusions can already be drawn, and it is worthwhile to set them out at this point.

(1) The techniques of measurement chosen work well for most of the materials being studied. End measurements are reproducible even on the softest of the specimens. Measurements of plastic strain are acceptable on all of the metals except the titanium alloy, the elastic properties of which exceed those of the gages. This material will require an alternate testing method, and efforts are being made to improve the reliability of the capacitance extensometer to meet this need. The aluminum oxide has caused measurement problems because of its sensitivity to eccentric loading, and these are being minimized by a change in the gripping assembly.

(2) The microyield stresses measured are consistently below those reported in the literature. The present numbers are believed to be more accurate as a result of increased refinements of the equipment and methods used. In particular, the special care taken in handling specimen surfaces is believed to have been largely responsible for the more realistic but lower values.

(3) The potential influence of machined surfaces on precision mechanical properties and on dimensional stability is apparent in the residual stress experiments. Because the samples are already exposed to an internal stress, any external stresses must be added to those. Thus, the measured external stress is only a part of the force affecting the experimental results as measured on a machined sample.

(4) Transmission-electron microscopy is proving to be a tool of considerable value in evaluating the mechanisms of microstrain. It appears that dislocations tend to generate at discontinuities (such as precipitates) at grain boundaries, then propagate through the grain. Tangles, as such, do not seem to result from microstrain. This suggests, at least in principle, that higher microyield stress values can be obtained in small grain structures wherein the grain boundaries are free of precipitates. This emphasizes the point that micromechanical properties are not necessarily optimized by the same processing and heat treatment that would provide the best macromechanical properties.

FUTURE WORK

Emphasis during the first year's research was placed on determining the micromechanical properties of the materials being studied. The second year's effort will be devoted mainly to the dimensional stability aspects of the program. The machining studies will be continued, and the experiments concerning the effects of plastic strain, and load and thermal cycling on dimensional stability will be conducted.

Micromechanical property tests will be continued to further study the phenomena of microstrain hardening and recovery of microstrain and the mechanisms of microplastic deformation. The microyield stress of Ti-5Al-2.5Sn, beryllium, and Al_2O_3 will be determined. Dead-weight load, microcreep tests also will be conducted for all of the materials being studied.

REFERENCES

1. Schetky, L. M., "The Properties of Metals and Alloys of Particular Interest in Precision Instrument Construction", R-137, MIT Instrumentation Laboratory (January, 1957).

2. Davies, R. G., and Ku, R. C., "Solid-Solution Strengthening in Iron-Base Alloys", Trans. AIME, 236, 1691 (December, 1966).

Unclassified

Security Classification

DOCUMENT CONTROL DATA - R&D

(Security classification of title, body of abstract and indexing annotation must be entered when the overall report is classified)

1. ORIGINATING ACTIVITY (Corporate author) Battelle Memorial Institute	2a. REPORT SECURITY CLASSIFICATION Unclassified 2b. GROUP

3. REPORT TITLE

Study of Microplastic Properties and Dimensional Stability of Materials

4. DESCRIPTIVE NOTES (Type of report and inclusive dates)
Summary Report; June 1, 1966 to May 31, 1967

5. AUTHOR(S) (Last name, first name, initial)

Ingram, Albert G., Maringer, Robert E., Holden, Frank C.

6. REPORT DATE	7a. TOTAL NO. OF PAGES	7b. NO. OF REFS
May 31, 1967	72	2

8a. CONTRACT OR GRANT NO. AF 33 (615)-5218 b. PROJECT NO. c. d.	9a. ORIGINATOR'S REPORT NUMBER(S) 9b. OTHER REPORT NO(S) (Any other numbers that may be assigned this report)

10. AVAILABILITY/LIMITATION NOTICES

11. SUPPLEMENTARY NOTES	12. SPONSORING MILITARY ACTIVITY Air Force Systems Command Wright-Patterson Air Force Base Ohio

13. ABSTRACT

Microyield stresses of 39-40 ksi for Ni-Span-C, 69-70 ksi for 440 C stainless steel, and 7.5 ksi for A 356 cast aluminum have been determined. Microyield stress tests are in progress for Ti-5A1-2.5Sn, beryllium, and aluminum oxide. Experiments have shown that residual strains of 20-40 μ in./in. increase the microyield stress, but a small fraction of this increase is lost upon allowing the specimen to recover at room temperature for up to 24 hours. Electron microscope studies indicated that microplastic flow in Ni-Span-C is the result of dislocation generation at second phase particles in grain boundaries. For A 356 cast aluminum, the generation of interfacial dislocations at Mg_2Si particles appeared to be the controlling mechanism.

Experiments are being conducted to determine, and eventually minimize, the residual stresses introduced by machining in all of the materials being studied. In addition, the effects on dimensional stability of load and thermal cycling, and plastic strain are being investigated.

A prototype capacitor strain gage has been constructed. The design is currently being modified to eliminate slippage of the page elements as the specimen is loaded and unloaded.

DD FORM 1 JAN 64 1473

Unclassified

Security Classification

14. KEY WORDS	LINK A		LINK B		LINK C	
	ROLE	WT	ROLE	WT	ROLE	WT
Microplastic Properties						
Microstrain						
Microyield stress						
Precision elastic limit						
Dimensional stability						
Titanium						
Stainless steel						
Beryllium						
Aluminum						
Invar						
Aluminum Oxide						